Fluxes of CO_2 from natural seep sites and Sleipner storage site

Peter Linke, Matthias Haeckel, Jens Schneider v. Deimling, Lisa Vielstädte, Mark Schmidt, Stefan Sommer, Jens Karstens, Christian Berndt, Hauke Herreilers [1]

Anna Lichtschlag, Douglas Connelly [2]

Rachael James, Melis Cevatoglu [3]

Tamara Baumberger, Rolf Birger Pedersen, Alden Ross Denny, Hans Tore Rapp, Ingunn Hindenes Thorseth [4]

Massimiliano Molari, Dirk de Beer [5]

Gregor Rehder, Stine Kedzior [6]

Stanley Beaubien [7]

Cinzia De Vittor [8]

[1] Helmholtz Centre for Ocean Research Kiel (GEOMAR)

[2] Natural Environmental Research Council (NERC-NOCS)

[3] University of Southampton (SOTON)

[4] Centre for Geobiology, University of Bergen (UiB)

[5] Max Planck Institute for Marine Microbiology Bremen (MPI)

[6] Leibniz Institute for Baltic Sea Research (IOW)

[7] University of Roma (Uni Roma1)

[8] National Institute of Oceanography and Geophysics (OGS)

Contents

1 Introduction

This document constitutes Deliverable 2.2 in the ECO_2 project and provides a geochemical report on fluxes of CO_2 from natural seep sites and the Sleipner storage site including measurements at abandoned wells and the Hugin fracture.

2 Natural analogs

Natural CO_2 seeps in the Okinawa Trough, at the Jan Mayen and Panarea gas seeps and the Salt Dome Juist area were studied as analogs for CO_2 leakage allowing in situ investigation (e.g. hydro-acoustic, gas and geochemical flux measurements) of a number of key processes controlling leakage pathways and impacts on biota.

2.1 Okinawa Trough

As explained in earlier progress reports, the originally planned additional field work in the Okinawa Trough had to be cancelled despite successful application of ship time due to severe underfunding of equipment. Therefore, according to what has been stated within the progress reports, data from an earlier cruise in the Okinawa Trough (expedition SO 196 of the German RV SONNE, 2008) were revisited to answer specific ECO_2-related questions. However, as no new field work was performed, experiments designed specifically to match approaches followed within ECO_2 could not be executed. However, several results in the line of the overarching question of deliverable 2.2 can be addressed.

The Okinawa Trough is one of two known back arc basins worldwide where liquid carbon dioxide is emitted from the seafloor into the water column. While the first encounter with sub-sedimentary liquid CO_2 in the Okinawa Trough was in the Jade hydrothermal field (Sakai et al., 1990), recent investigations focus on two hydrothermal fields in the south-western part of the Okinawa Trough, the Yonaguni Knoll IV and the Hatoma Knoll field.

The Yonaguni Knoll IV hydrothermal field (24° 50.9’ N, 122° 42.0’ E, Fig. 1) comprises a sedimentary valley with a length of about 1000 m, width of 500 m and a maximum water depth of 1385 m, surrounded by large piles of rock debris, enclosing a string of active hydrothermal vents. Seven active

venting sites have been identified at the Yonaguni Knoll IV field, named Lion, Crystal, Tiger, and Swallow chimney, Abyss vent, Carp, and Mosquito chimney (from north to south) (Gena et al., 2005), which partially emit hot fluids with temperatures up to 330°C from black and clear smoker vents. Emissions of cold liquid CO_2 were observed south of Tiger and northeast of Swallow chimney (Konno et al., 2006). Particularly important for the scope of ECO_2, Yonaguni Knoll IV hosts one of the few sites on Earth know where liquid CO_2 leaks through thick layer of terrigeneous sediments (Inagaki et al., 2006).

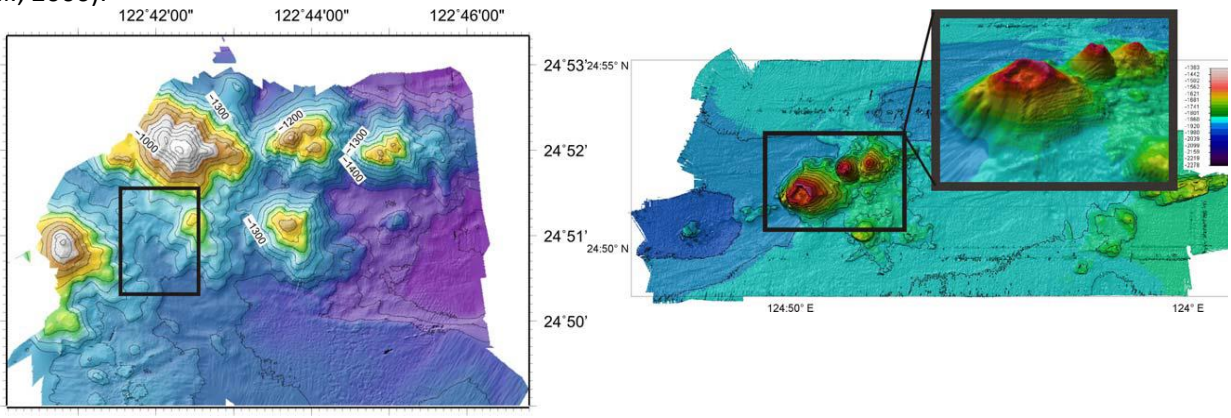

Fig. 1: Bathymetric charts covering the CO_2-rich hydrothermal fields of the Okinawa Trough. Left: Yonaguni Knoll IV; Right: Hatoma Knoll. The highlighted areas are the main fields of investigation.

Hatoma Knoll is a submarine volcano located 60 nm to the east of Yonaguni Knoll IV (24° 51.3' N, 123° 50.5' E, Fig. 1) at a depth of about 1530 m. The approximately 120 m high and 400 m wide caldera is almost completely closed except for a small outcrop at the southern rim, probably resulting from a former flank collapse and slumping (Rehder and Schneider von Deimling, 2008; Shitashima et al., 2008). A total of at least twelve hydrothermal vents has been identified at the Hatoma Knoll. They are located in the middle of the caldera close to a round-shaped 30 m high mound, and at the north-western rim of the caldera. The highest hydrothermal activity at Hatoma Knoll is located in the center of the caldera.

2.1.1 Hydro-acoustic measurements

Bathymetric mapping using the hull-mounted KONGSBERG EM120 revealed the recent morphology of the seafloor that has not undergone significant change since the last measurement presented by Konno et al. (2006). In the year 2008, the KONGSBERG multibeam system did not allow for recording the water column for detection of fluid/gas venting. Therefore, the hull-mounted PARASOUND system was used for water column imaging as well as sub bottom investigations during SO 196. One indication about a rising water column feature potentially represents gas/fluid rise through the water column (Fig. 2). However, the feasibility of ship born sonar was limited for hydrothermal vent imaging due to side-lobe signals partially crossing into the 'silent' water column acoustic domain caused by the steep slopes surrounding the vent sites.

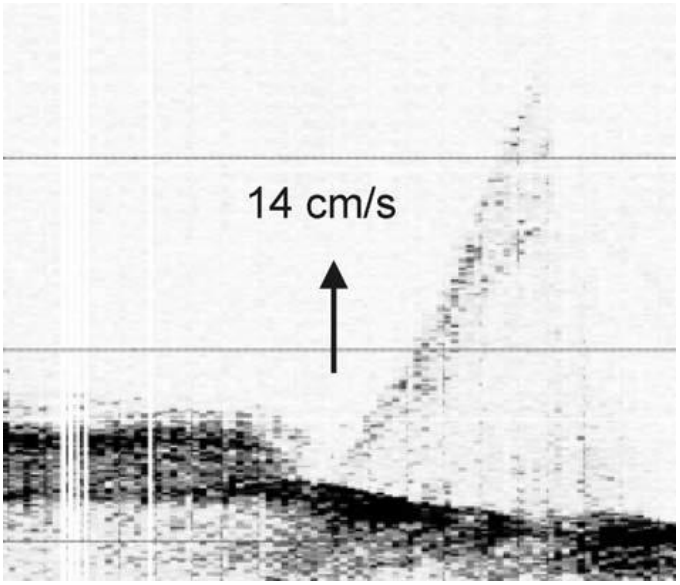

Fig. 2: 18 kHz water column reflection recorded by PARADIGMA. Data pattern indicates a rising reflector.

Several PARASOUND profiles have been recorded in the vicinity of active chimneys to better constrain the subsurface sediment character. Outside of the venting area the subbottom records revealed distinct layering with a maximum penetration of around 50 m (Fig. 3). On the right side of figure 3, acoustic blanking is visible in the Hatoma Knoll field; its origin is unknown and was not further constrained, because it was recorded off the area of interest.

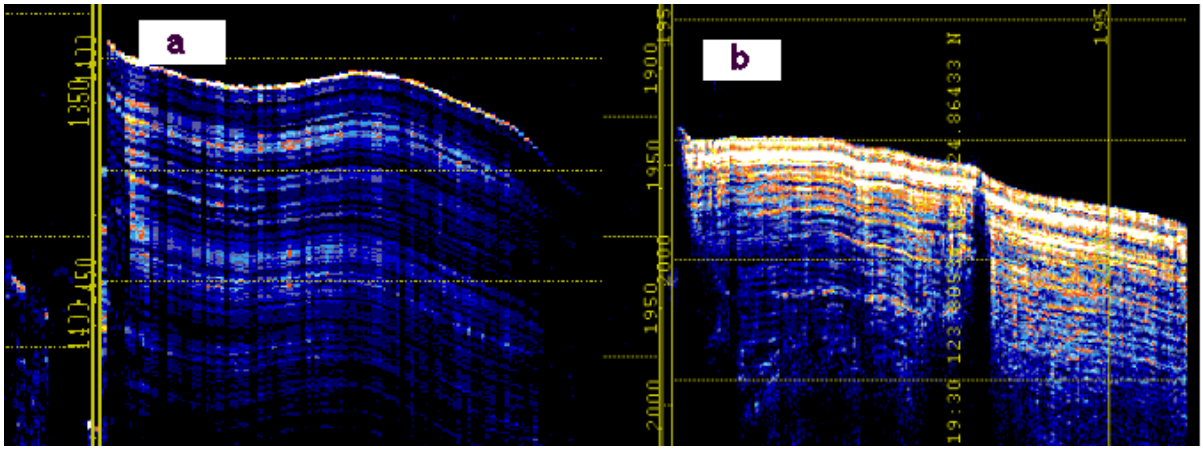

Fig. 3: Parametric echogram in the reference/off-study area of the Yonaguni (a) and Hatoma (b) Knoll areas.

Within the chimney environment of Yonaguni Knoll IV acoustic penetration appeared limited to only a few meters. Locally, a profound transition from weak to strong surface scattering could be observed (Fig. 4). From visual inspection (TV MUC, ROV) and coring it was found, that the upper sediment is mostly very soft. Thus, we suggest a shallow, subsurface structure (potentially containing free gas or liquid CO_2) caused the enhanced scattering and reduced acoustic penetration.

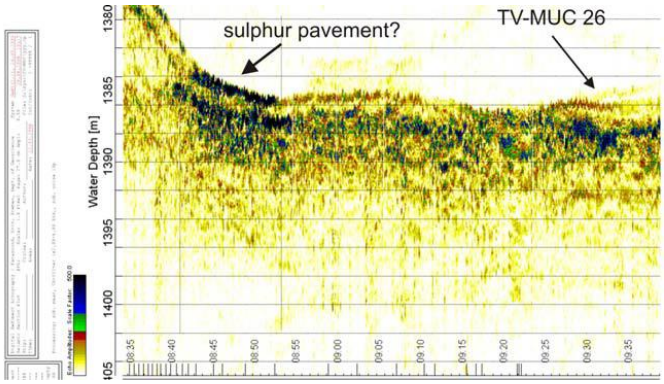

Fig. 4: Parallel recording of Parasound data during TV MUC-26 track in the swallow chimney area.

2.1.2 *Gas fluxes in the water column*

The field observations showed variable CO_2-rich vent types both in the Yonaguni Knoll IV field as well as in the Hatoma Knoll vent field, including the release of droplets of a liquid phase with CO_2 as the main component, gaseous phases with higher fractions of methane, as well as release of CO_2-rich hot hydrothermal fluids (Rehder and Schneider v. Deimling, 2008). Analysis of the water column data gathered at both sites, comprising 25 CTD stations (11 at Hatoma Knoll, 14 at Yonaguni Knoll IV), equipped with pH and Eh sensors as well as two LADCP (upward-downward looking in a master/slave configuration), show a dominant influence of the hydrothermal fluid on the (excess) CO_2-contribution in both working areas. Measurements of total CO_2 (TCO_2) and dissolved He and its isotopes reveal a linear relation of excess ^3He and excess CO_2, with clearly distinct slopes in both regions. In brief, the data suggest a minor importance of the liquid (condensed) CO_2-rich phases for the overall CO_2 release, an almost entirely CO_2-flux driven perturbation of the pH field with negligible contribution of other acids, and higher CO_2 enrichment ($CO_2/^3He$ ratio) of the main fluid source at Hatoma Knoll than compared to Yonaguni Knoll IV. The data from Yonaguni Knoll IV also indicate a hitherto unknown source in the northeastern flank of the valley hosting the so far known hydrothermal vents. These findings will be summarized in a manuscript which will be submitted soon (Kedzior et al., in prep.).

Due to the large variability of the current patterns in the working areas, in particular in the Yonaguni Knoll IV field, an assessment of the CO_2 flux based excess CO_2 inventory and current field has proven to be difficult. Calculation of a rough estimate of CO_2 flux is planned based on an approximation of the heat flux derived from plume propagation theories. Maximum rise height of the plumes yielded a total heat flux of 540 MW and 82 MW for the Yonaguni Knoll IV and Hatoma Knoll research areas, respectively (Buß, 2011). However, the lack of a well-defined heat-^3He (or heat-TCO_2) signature will put constraints on the accuracy of this approach.

2.1.3 *Geochemical flux measurements*

The flux of geochemical constituents through the sediments around the CO_2-rich Abyss Vent, Yonaguni Knoll IV, Okinawa Trough, was investigated using the integrated analysis of the data obtained from the deployments of a microprofiler, a multicorer, gravity corers, and ROV-operated push coring (de Beer et al., 2013). Abyss Vent is a sedimentary venting site characterized by a few holes in the seafloor emitting hot fluids. The microprofiler was deployed at a total of 5 stations with a distance from 0.5 to 500m from the main vent (the latter served as a reference station). Data were gathered during expedition SO 196 of RV SONNE, as well during JAMSTEC NT10-06 Leg 3 cruise with RV Natsushima in 2010. Calculated flux of dissolved CO_2 in this area was estimated between 30 and

300 x 10^{-8} mol m^{-2} s^{-1}, and was in accordance with a purely diffusive driven escape from the CO_2-rich sediments, with an estimated sediment depth of 20 cm to reach full CO_2 saturation (1000 to 1700 mM). Local diagenetic processes appeared to be of minor importance for the fluxes of all constituents, apparently caused by low microbial activity. De Beer et al. (2013) reason that this might be caused by external H_2CO_3 levels too high to maintain cellular pH homeostasis (see also 2.1.4).

2.1.4 Impact of CO_2 and other geochemical species on biological communities

In addition to the mineral chimneys through which hot fluid (>300°C) escapes, pavements of elemental sulphur and amorphous SiO_2 precipitates were observed within the Yonaguni Knoll IV hydrothermal field, associated with holes and cracks in the underlying soft sediments from which hot fluid and liquid CO_2 emanated. The pH profile became steeper close to the vent (100 m), showing a pH of ca. 4.5 >6cm below the seafloor. Porewater profiles showed elevated concentration of sulphide, methane, ammonium, manganese and iron, which may serve as electron donors for microbial oxygen consumption (De Beer et al., 2013). The benthic chamber measurements showed rather low total oxygen consumption rates at and near the vent sites which were, however, higher than at the reference site (data in preparation for publication). Generally, both sulphate reduction (SR) and anaerobic methane oxidation (AOM) were found to be higher close to the vents than at the distant site >20 m away. These findings provide evidence that the constituents of the hydrothermal fluid fuelled these microbial processes, even under the conduction of high CO_2 concentration and low pH associated with the vents. However, SR and AOM were restricted to the upper 7–15 cm below seafloor, although neither temperature, low pH, nor the availability of methane and sulfate could be limiting microbial activity. We argue that the extremely high subsurface concentrations of dissolved CO_2 (1000–1700mM), which disrupt the cellular pH homeostasis, and lead to end-product inhibition.

Changes in benthic bacterial community composition were determined across a natural gradient in CO_2 leakage and pH using Automated Ribosomal Intergenic Spacer Analysis (ARISA) and 454 massively parallel tag sequencing. The distribution of bacterial populations was compared across different locations ranging from strongly CO_2 vented sites to background conditions in the sediment-hosted CO_2-seepage area within the Yonaguni Knoll IV field. The sampling sites grouped into three categories of CO_2 impact, 1) high CO_2 seepage, characterized by pH as low as 5-6 at the surface seafloor and strong alteration of the liquid and solid phase of the sediment matrix; 2) low to intermediate CO_2 seepage mostly confined to the subsurface (> 5 cm); and 3) background conditions, indicated by absence of CO_2 venting (Fig. 5). A CO_2 impact on bacterial diversity was recognized, from phylum to genus and individual tag sequence levels. Bacterial richness decreased significantly with increasing CO_2, and dissimilarity between bacterial communities increased with increasing CO2 concentration. Members of the acidophilic Deltaproteobacteria and hydrothermal vent Epsilonproteobacteria increased in sequence abundance with higher CO_2 leakage. In contrast, the sequence abundance of Alphaproteobacteria and Planctomycetes decreased, which might indicate sensitivity of some deep-sea bacterial taxa to CO_2 venting (Neumann 2012, data in preparation for publication).

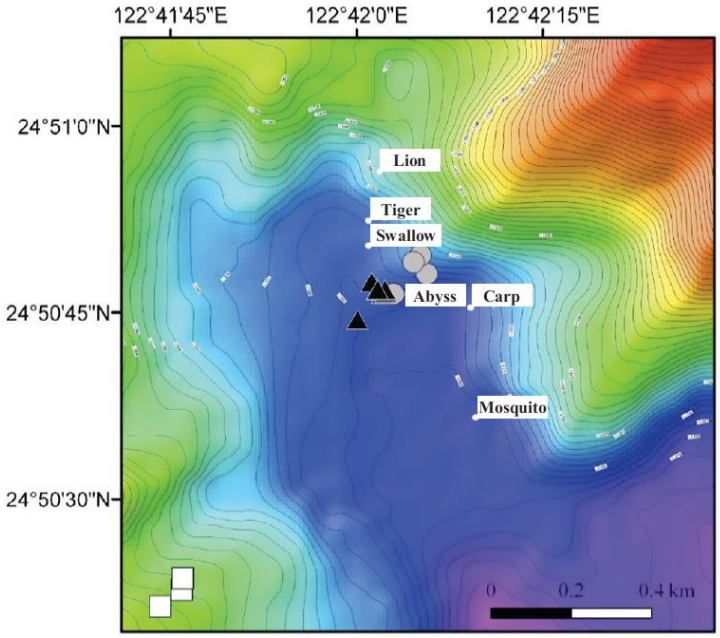

Fig. 5: Overview of the Yonaguni Knoll IV hydrothermal vent system. Symbols for sediment samples of the macro/meiofauna study are white squares for background, black triangles for high CO_2 seepage, and grey circles for low CO_2 seepage sites. Stations for the benthic community pattern study are on the same regional pattern (in most cases identical).

Metazoan macrofaunal and meiofaunal communities were examined using a similar classification of CO_2 seepage influence. Abundance, distribution patterns and richness of macro- and meiobenthic communities were quantified. Macro- and meiofauna showed different responses to elevated CO_2 concentrations in porewaters. The macrofauna was dominated by polychaetes, crustaceans and gastropods in the Background area with lower abundances at the CO_2 impacted habitats. In contrast, high abundances of juvenile bivalves were detected in the High CO_2 seepage habitat. Meiofauna communities were dominated by nematodes, and were similar in abundance and structure at the background and Low CO_2 seepage areas, but differed substantially at High CO_2 seepage. One specific nematode genus Thalassomonhystera dominated all three habitats and showed highest densities at High CO_2 seepage, along with several other nematode taxa. Our study of a CO_2-leaking deep-sea ecosystem shows substantial effects of seafloor acidification on macrofauna and meiofauna community composition, such as local losses and replacement of CO_2-sensitive taxa. Ecosystem surveys for the assessment of potential ecological risks of Carbon Capture and Storage in the deep seabed must include high-resolution biodiversity studies in relation to biogeochemical gradients (Neumann, 2012; Yanagawa et al., 2012).

2.2 Jan Mayen Gas Seeps

The R/V G.O. Sars cruised to the Jan Mayen vent fields in the summer of 2011, 2012 and 2013. A main feature of the Jan Mayen vent fields is the high CO_2 concentrations of the venting high-temperature fluids as well as the release of CO_2 bubbles. CO_2 concentrations of up to 113 mmol/kg were measured in the fluids.

2.2.1 Hydro-acoustic measurements

Both cruises, in 2012 and 2013, collected multibeam (MBES) and single-beam echosounder (SBES) profiles over the main Troll Wall vent field, making passes both parallel and perpendicular to the cliff face that comprises the Troll Wall field. The 2012 data was somewhat compromised by the concurrent use of an EK60 single beam echosounder without a timing delay system resulting in systematic interference of the multibeam system, especially in the water column image. The 2013 data collection, though hampered for most of the time by high winds and large NE swell, collected numerous passes of high quality water column returns of the Troll Wall bubble plumes, giving clear indication of their rise heights, plume structure, and occurrence of plumes along the Troll Wall venting system (Figs. 6 and 7).

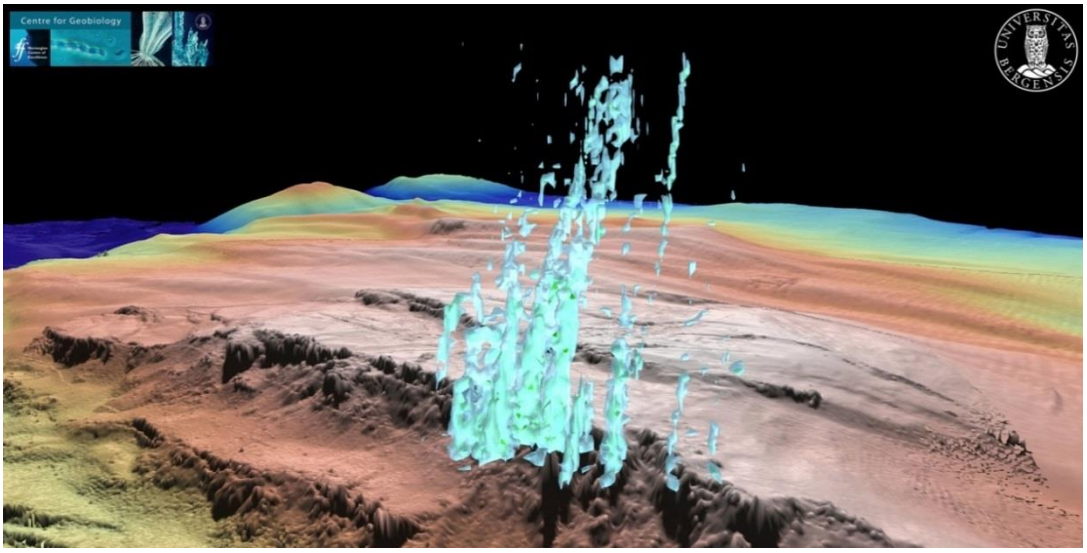

Fig. 6: Image of the Troll Wall venting system, as a compilation of several MBES survey lines and gridded as an iso-amplitude volume.

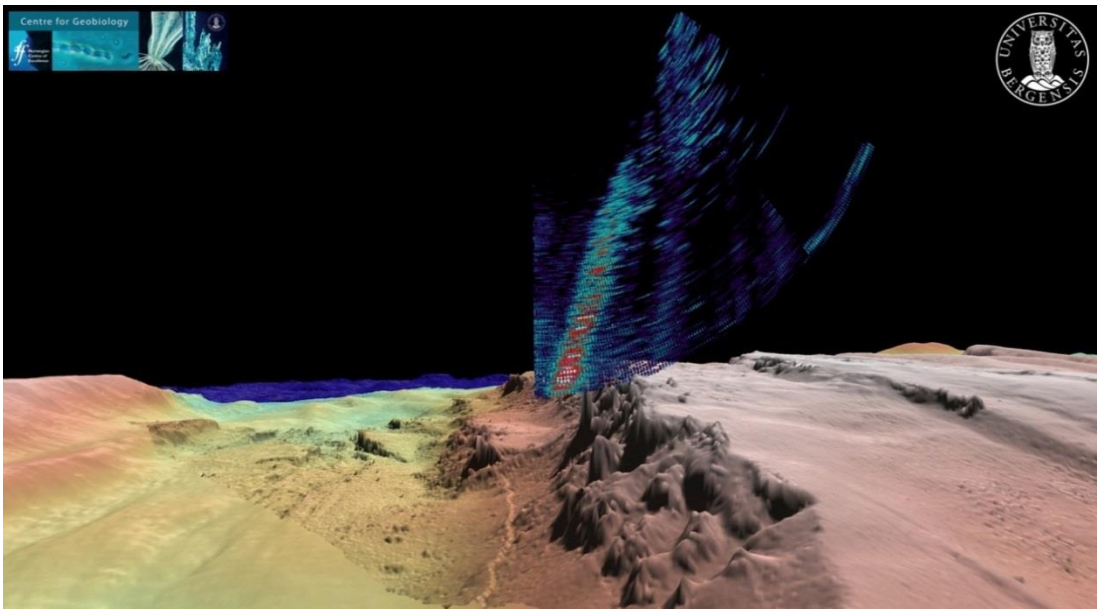

Fig. 7: Single ping profile of the Troll Wall venting system demonstrating the horizontal resolution achievable with MBES and the plume shapes that can be seen with this system.

From the Jan Mayen vent fields is clear that MBES is a powerful tool for determining the occurrence and dynamics of bubble plumes in the water column. Given the dramatically improved survey swath provided by MBES over SBES, the MBES is much more efficient in surveying for seafloor gas seeps. In addition to locating the seeps the concurrent acquisition of bathymetric soundings provides a detailed look at the seafloor features that may be related to the gas seeps. SBES systems are appropriate for examining time-series on a single location, and could be used to calculate the rise velocity of bubbles from a single source, but given the narrow water column region surveyed by the single beam these systems are not appropriate for locating gas seeps on the seafloor.

While MBES systems are powerful tools for locating seafloor gas seeps, they work best on dedicated water column surveys and are highly susceptible to interference from other acoustic systems. MBES surveys run concurrent with SBES systems must be set up with timing offsets to prevent signal interaction. As well, it is not possible to run MBES and sub-bottom profiling parametric systems concurrently. With these stipulations, multibeam sonar systems have the potential to provide the highest resolution, fastest, and consequently least expensive method for monitoring for potential gas seeps possible with current technologies.

2.2.2 Gas fluxes in the water column

During the expedition in 2011, a new tool for sampling gas bubbles emanating from the seafloor in diffuse flow areas was successfully tested and subsequently used for sampling. The collection of vent fluid and gas bubble samples at these diffuse flow locations and also at focused flow, high-temperature (up to 270°C) vent structures allows us to determine the CO_2-content of fluids exiting the seafloor at the JMVF. Figure 8 shows the gas composition of gas bubbles exiting the seafloor in a diffusive venting area at Trollveggen (JMVF). Carbon dioxide is the major gas component in these gas bubbles. In addition, Jan Mayen high-temperature vent fluids have CO_2 concentrations of up to 113 mmol/kg (at the high end for mid-ocean ridge systems), but low H_2, H_2S and CH_4 concentrations. This high CO_2 release into the water column allows for investigations of chemical fluxes from the seafloor into the water column and to describe the impact of CO_2 on biological communities.

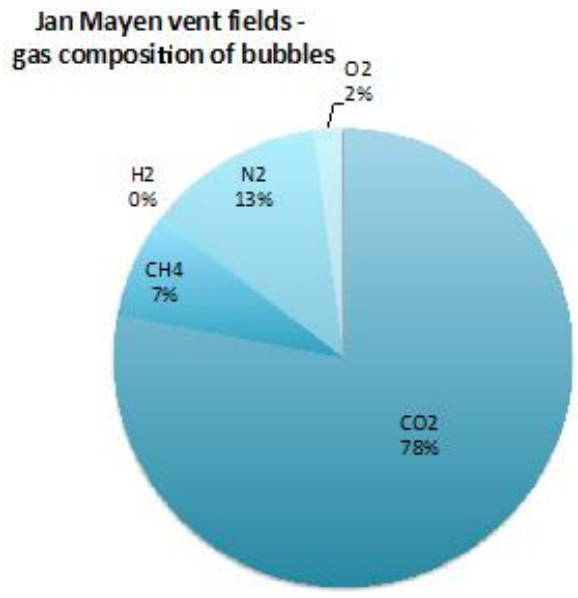

Fig. 8: Gas composition of a gas bubbles collected in dive GS11-ROV04 at Trollveggen (Jan Mayen vent fields).

In addition to obtain samples for fluid and gas composition, important observations were made regarding the formation and dissociation of CO_2-hydrates. During the expedition in 2011, video imaging documented the dissociation of CO_2-hydrates (Fig. 9) during the ascent of the (remotely operated vehicle (ROV). Starting with gas hydrate only at about 550 m water depth, some bubbles were released from the hydrate at about 430 m water depth. Nevertheless, at a depth of about 120 m, big bubbles started to build from the hydrate and at 80 m water depth the major amount of hydrate vanished within very short time. From the gas composition analysis it is known that the main component of this gas hydrates is CO_2.

Fig. 9: Dissociation of CO_2-hydrate sampled at Trollveggen (JMVF) during the ascent of the ROV.

During the research cruise in 2012, gas hydrate formation at a hydrothermal chimney was observed. Within a distance of a few centimeters, high-temperature vent fluid venting and cold CO_2-hydrate formation was ongoing simultaneously. High-temperature fluids cooled down to background seawater temperatures right at the chimneys moving the fluid into the stability field of CO_2 hydrates. This explains the observation of bubbles with hydrate skins rising from chimney walls at the JMVF. A very steep temperature gradient between the main orifice opening (where the high-T fluids were sampled) and the chimney walls (hydrate-coated bubbles were sampled) must thus be present.

2.2.3 Geochemical flux measurements

Carbon dioxide concentrations of the high-temperature vent fluids were used to estimate the CO_2-flux into the water column at the JMVF. For the flux estimation, an average dissolved CO_2 concentration of 100 mmol/kg was used, and it was assumed that endmember fluids showing lower concentrations had been degassed by giving rise to CO_2 bubbles. Therefore, there is no need to estimate the flux of CO_2 as bubbles. The number of venting chimneys (about 40) was determined from video observations from the ROV. The number of chimneys in combination with the venting rate of approximately 10 l/s per orifice and the determined CO_2 concentration results in an estimated CO_2 flux of about 900 t/y at the JMVF. Setting this into context with the CO_2 concentrations in the water column, it shows that the local (0.5 to 1 km^3) yearly input of CO_2 from the vent field into the water column is about 2 % of the water column CO_2.

2.2.4 Impact of CO_2 and other geochemical species on biological communities

Recent studies of the benthic ecosystem surrounding the hydrothermal vents on the Mohn-Ridge have resulted in some unexpected discoveries. The benthic fauna is exposed to the CO_2-rich hydrothermal fluids emitted from the chimney systems or as more diffuse seeping in soft sediments surrounding the vents, and organisms with delicate calcareous skeletons were not expected to thrive under such conditions. During the 2011 and 2012 cruises we collected material and photographed a highly diverse fauna of calcareous sponges on hard substrates surrounding the vents. Calcareous sponges have very delicate skeletal structures and are expected to be among the first that will suffer from ocean acidification. Here these organisms were directly exposed to the CO_2-rich fluids, and interestingly, they do not seem to be impacted by the high CO_2 concentration in the surrounding waters (Fig. 10). More detailed studies of the skeleton structures in these sponges are now being made, and molecular tools are used to investigate if the expression of genes involved in skeletogenesis in calcareous sponges in vent systems is different than in background waters.

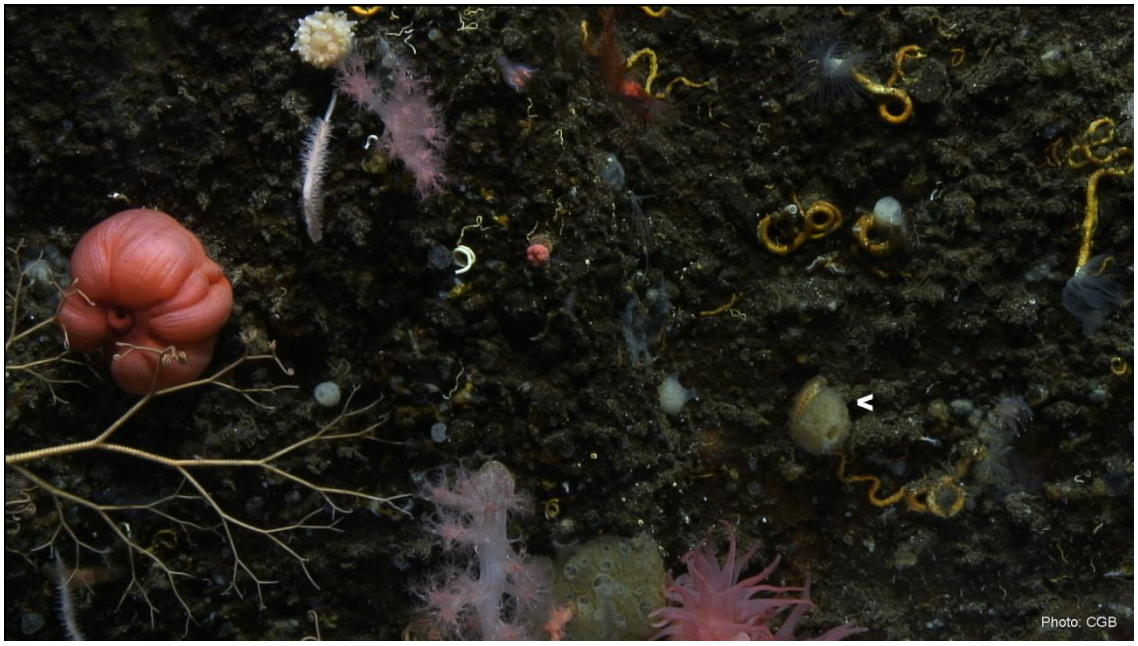

Fig. 10: Benthic fauna from a dead chimney structure at the Jan Mayen vent field. Arrow head indicates an individual of a new and highly abundant species of calcareous sponges from the area.

2.3 Panarea Gas Seeps

The island of Panarea (Aeolian Islands, Italy) lies to the north of Sicily (Fig. 11) and is well known for the large volumes of natural, magmatic CO_2 leaking from the seafloor on a shallow water platform just to the east of the main island. Based on the range of water depths and different gas leakage rates, as well as its close proximity to shore, the Panarea site represents an exceptional location to study the fate and transport of CO_2 in the water column and to test new leakage monitoring technologies.

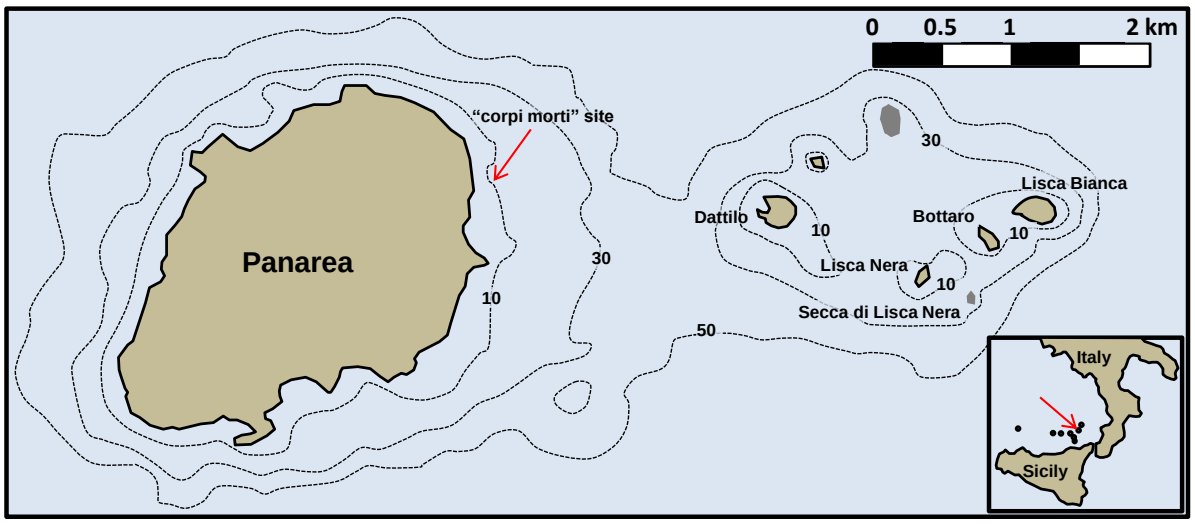

Fig. 11: Location map of the Island of Panarea and the associated islets to the east, where the well-known, shallow water CO_2 emission sites are located.

The leaking CO_2 is released most strongly in the area near two islets located 3 km to the east of Panarea (Lisca Bianca and Bottaro; Fig. 11), in waters that are 5 to 30 m deep. This natural CO_2-release field (ca. 3 km^2) has been active for centuries, with gas emanating from a series of NW-SE and NE-SW trending fractures (Esposito et al., 2006). In the early 1980's researchers began to conduct gas geochemistry surveys of the area (Caliro et al., 2004), showing that the system was relatively stable in both gas chemistry (e.g. 98% CO_2, 1.7% H_2S plus other trace gases) and fluxes (7-9 x 10^6 l/d). On November 2 and 3, 2002, a gas outburst event formed pockmarks and increased the total gas flow rate by about 2 orders of magnitude (4 x 10^8 l/d) (Caliro et al., 2004), with large volumes of gas reaching the water surface. Fluxes began to decrease towards pre-outburst conditions about 3 months after the event. Most release points emit gas only, although some also release water of different origin, ranging from geothermal to seawater end-members that are mixed to variable degrees (Tassi et al., 2009).

2.3.1 Hydro-acoustic measurements

While these shallow gas discharge sites are well known, only recently further gas discharge sites at about 70 – 80 m water depth were discovered during a cruise with RV Urania in 2011 (McGinnis et al., 2011a) and a previous cruise with RV Poseidon in 2006 (Monecke et al., 2012). Acoustic evidence of rising gas bubbles (flares) at about 80 different locations and elevated surface concentrations in methane and carbon dioxide were found throughout the surveyed area.

For a quick review, data were analysed in QPS-Fledermaus/FMMidwater to illustrate the maximum gas bubble rise and flare height, respectively. Assuming almost pure CO_2 gas being released from

the seafloor (based on ROV sampling), this rise height would suggest that most of the CO_2 has been dissolved and replaced by stripped oxygen and nitrogen (McGinnis et al., 2011). But the significant rise height has major implications on the acoustic detection probability that scales to a certain degree to the flare rise height, especially in the presence of fish as a main driver for misinterpretations between bubbles and fish. Individual gas bubble "chains" escaping from the seabed could be imaged in great detail using high-frequency acoustic multibeam echosounder data (Fig. 12).

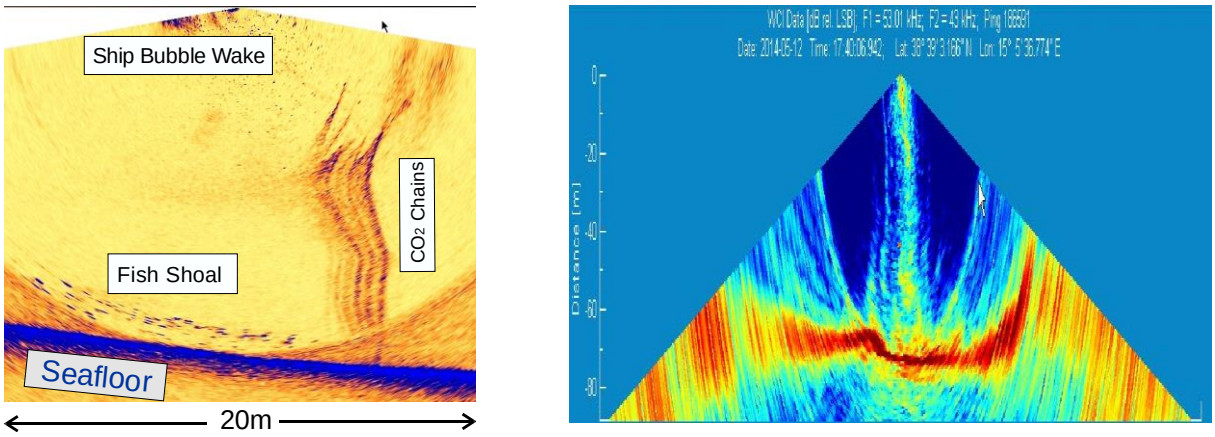

Fig. 12: (left) Natural release of CO_2 from the seabed (Panarea, Italy) recorded with 400 kHz (R2Sonic 2024). (right) 70 m deep gas release recorded with ELAC SB3050 at 50 kHz.

Using such high-frequency multibeam acoustics even allows to estimate rise velocities of gas bubbles as described in Schneider von Deimling and Papenberg (2012). During the recent cruise POS469 in May 2014 (Linke, 2014) we used a 50 kHz system also providing insight into the interior structures of the gas flares. Therefore, stationary multibeam data were acquired with a maximum ping repetition rate. Subsequently the data were loaded into MATLAB, threshold- and lowpass- filtered, gridded with a 3D interpolation scheme to obtain a 3D data cube. Individual slices through the 3D cube are presented in figure 13 revealing interior features like current-induced flare deflection and – if successive pings being evaluated over time – revealing vertical rise speed of individual "bubble clusters" as suggested in Schneider von Deimling and Papenberg (2012). Moreover, the general decay of the integrated acoustic energy as a rough indicator for the amount of gas bubbles and respective size distribution across the plume can be assessed by horizontal slices (Fig. 13).

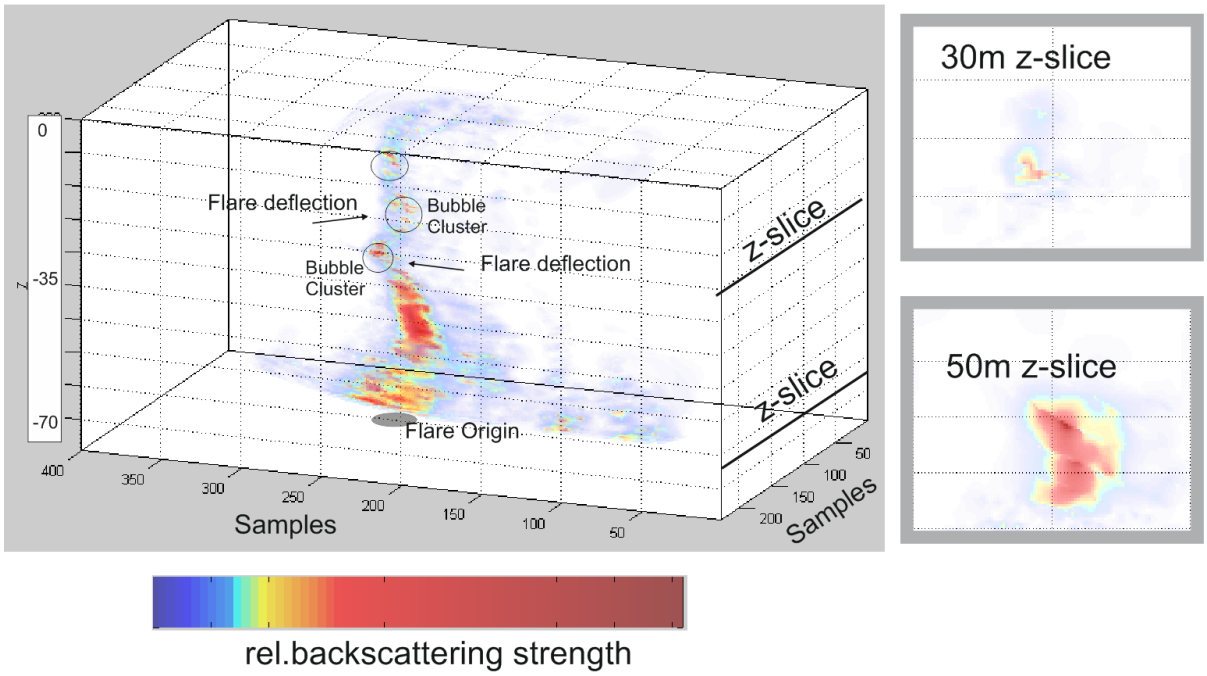

Fig. 13: 3D gridded and filtered data cube from ELAC SB3050 data. One sample is 0.2m in length. Inlets on the right side represent horizontal slices through the 3D cube for the assessment of plume width and integrated acoustic energy. The plume reaches 70 m high with maximum width of 6.5 m.

Near-range acoustic and visual gas bubble imaging

Acoustic imaging by multibeam clearly revealed that some of the gas bubbles rise up to the sea surface. By using a ROV mounted high-frequency sonar this observation was refined and the tempo-spatial evolution and extent of the rising plume could be mapped during cruise POS469. Therefore an ROV uplift experiment was conducted. The ROV was positioned 6 m downstream of the gas bubbles. During the first meters of uplift of the ROV pronounced backscatter from the seabed obscured acoustic water column scatterers like gas bubbles. Further upwards and some meters away from the seabed, a very pronounced acoustic signal was acquired and could be clearly cross-linked to the gas seepage site by a downward looking camera. The initial plume dimension could be measured online to 5.3 x 2.9 m^2 at 47 m water depth (Fig. 14a). By slow ROV uplift the bubble plume could be followed from the seabed up to the surface. Meanwhile the acoustic signal strength ceased but maintained up to the sea surface. At 16 m water depth the plume dimension was measured again to 4.3 x 2.0 m^2 (Fig. 14b).

Visually, the gas bubble plume got almost entirely lost only after a few meters of ROV uplift. We conclude that the majority of the gas volume got lost due to dissolution in agreement to Linke et al. (2012). However, a significant fraction of gas obviously survives as bubbles and rises through the water column spanning dozens of meters. This is considered an important finding, because acoustic gas bubble detection feasibility scales to a certain extent to the bubble rise height: if gas bubbles would rise only 5 m, then acoustic artefacts cannot un-ambiguously be discriminated against such seepages.

Enhanced vertical rise highly increases the acoustic detection feasibility and obviously the amount of remaining gas is high enough for distinct detection (Fig. 14b). Thus, even though bubbles at shallower

water depth might not contain CO_2 anymore, such bubbles still serve as a proxy for gas leakage at larger depth potentially releasing CO_2.

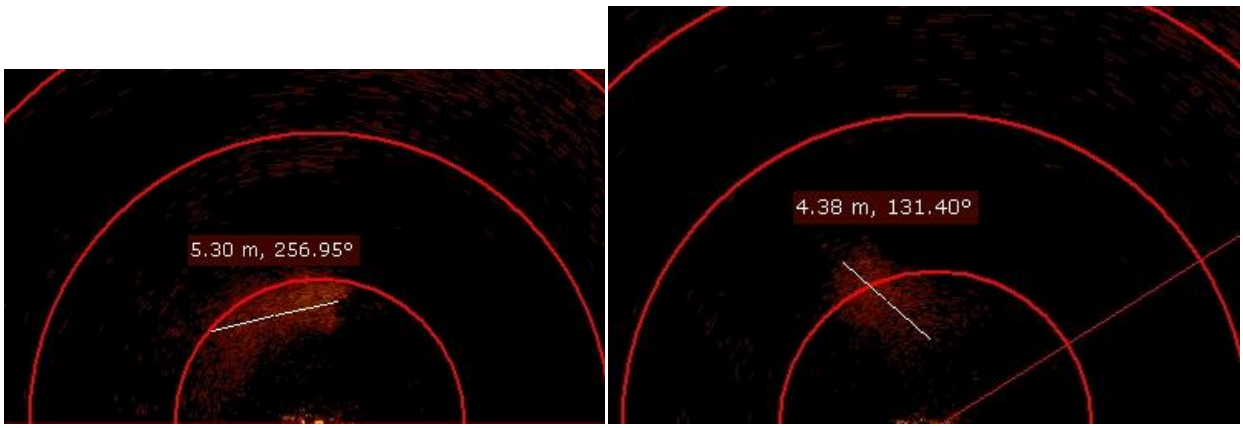

Fig. 14: Acoustic images gathered with the ROV mounted KONGSBERG MS 1000 with 200 kHz showing the bubble plume at (a) 47 m and (b) 16 m water depth with respective plume across dimension. Semi-circle distance is 3 m.

2.3.2 *Gas fluxes in the water column*

Gas fluxes from the sea floor to the overlying water column were measured by UniRoma1 and OGS at two different sites to the west of Bottaro Island (Fig. 15), "Bottaro crater" and "Point 21". Fluxes were calculated by measuring the time required to capture a given volume of gas (from 0.1 to 6 L) using a funnel of known surface area (0.17 m^2) and a graduated, inverted container (Fig. 15b). Results were converted to STP conditions to allow for a comparison of the volume flows at sites having different water depths, as well as a mass flux.

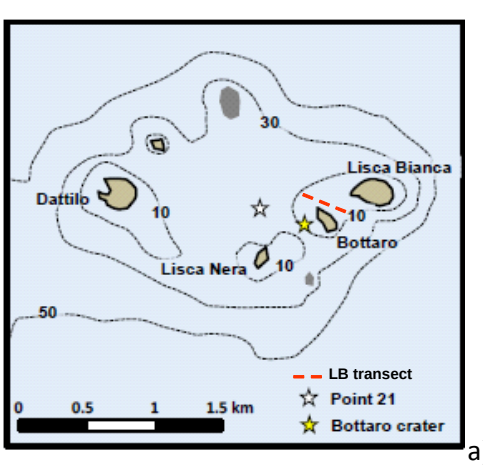

a)

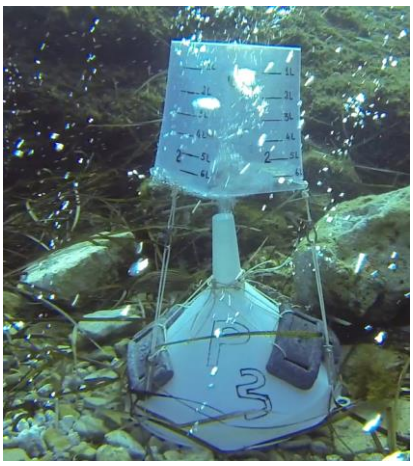

b)

Fig. 15: Location map of the two sites (a) where the rates of gas flux from the sea floor were measured using the accumulation chamber method (b). The positions of the 7 sampled stations are indicated as the LB transect (see chapter 2.3.4).

The area of the Bottaro crater is in 8-10 m deep water, with the base of the crater itself at a depth of about 11-12 m. The crater was subdivided into three different zones (Fig. 16a) based on the different leakage styles present: Zone 1 is a semi-circular area of uniform diffuse degassing (Fig. 16b); Zone 2 has isolated points of weak leakage; and Zone 3 has isolated points of moderate to stronger leakage that form bubble flares (Fig. 16c).

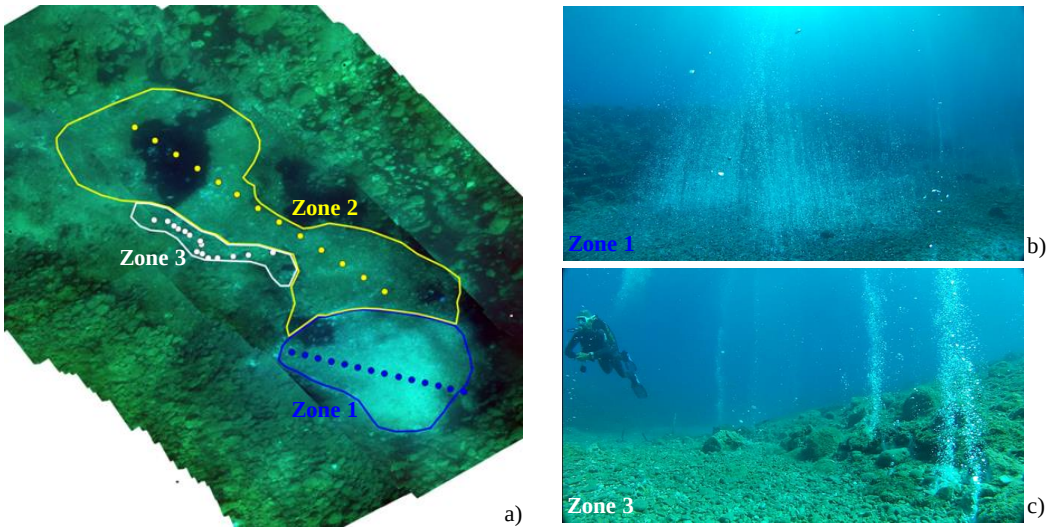

Fig. 16: Montage of video stills taken from the water surface showing the Bottaro crater and associated mapped zones (a). Photographs of representative leakage areas in Zones 1 (b) and 2 (c).

Measurements in Zones 1 and 2 were conducted along linear, regularly-spaced profiles which were placed irrespective of leakage points to obtain a representative statistical estimate of the average leakage rate. Sample spacing was 1 m and 2 m, respectively, and the average flux for each profile was multiplied by that zone's surface area to estimate total flow for that zone. In contrast, all major leakage points were measured in Zone 3 and all measured values were summed to calculate the total flux of this zone.

Table 1: Estimates of CO_2 leakage rates for the three measured zones within the Bottaro crater, given as both volume and mass flows.

	L_{STP} CO_2 / minute	T CO_2 / year	% total
Zone 1	336	323	82
Zone 2	3.9	3.7	1
Zone 3	70	68	17
Total	410	395	

The zone and total flows estimated using the above described approach are summarized in Table 1, which shows how the vast majority of the CO_2 leaking from the crater originates from the diffuse area of Zone 1 (c. 80%). It must be highlighted, however, that the assumptions made in extrapolating the individual point measurement results over the chosen surface area for that zone can influence the final calculated value. This was found to be particularly important for Zone 1, where slight changes in the number of points used (and corresponding surface area) could change the calculated flow by up to 50% (e.g. from 200 to 300 T CO_2 / yr). This is a common difficulty in extrapolating spatially variable data over a surface area, a source of error which could be minimised by capturing (and averaging) over a much larger area (e.g. 1 m^2 instead of the 0.17 m^2 used), although this creates logistical difficulties. Such a problem is not encountered with Zone 3, as leakage occurs from individual points that were measured and summed, and thus extrapolation was not necessary.

It is interesting to note, that whereas the diffuse degassing from Zone 1 is volumetrically the most important, the bubble flare from this feature does not rise as high in the water column as that observed for the individual points of Zone 3, some of which reached the water surface. This is due to the smaller average Zone 1 bubble size spread over a wider area, which allows for a more rapid dissolution. In contrast, the focussed flow from the moderate to strong individual vents results in larger bubbles that break-up and dissolve more slowly, which may allow for equilibration with O_2 and

N_2 in the water column thus stabilizing and prolonging the "life" of the rising bubbles. This could have important consequences for hydroacoustic monitoring, and the use of this technique to estimate leakage rates for highly soluble gases like CO_2 (as opposed to less soluble ones like CH_4).

GEOMAR investigated the same site on a yearly basis. As pointed out above, the gas flow at single points is highly variable in time and space ranging between 0.1 and 5.4 L min^{-1} at STP (1 bar and 298.5 K) within the diffuse seepage area. In contrast, gas emissions at the focused vents are far more constant at a maximum gas flow of 24.6 L min^{-1} ± 1.3 L min^{-1} at STP. The temporal variability of bulk gas emissions decreases to 24% and 2% at the diffuse site and at the focused vents, respectively. This might indicate that seeps are interconnected through subsurface channels, and thus variations in seepage activity at different locations are related to each other. This has also been observed at other seep sites (i.e. Coal Oil Point) by Leifer and Boles (2006), who simplified the relation of gas flux variability and seep fracture network in an electrical flow model. Total seabed emissions of the entire study site of 562 L min^{-1} (STP) or 0.6 kT CO_2 yr^{-1} are one order of magnitude higher than natural seepage rates at Tommeliten, a North Sea methane seepage area (i.e. 69 L min^{-1} (STP) or 26 t CH_4 yr^{-1}, Schneider et al.,2011).

The Point 21 site is located in deeper water, from 19 to 21 m, which, together with other work conducted at the site, limited the amount of time that the divers could conduct measurements. This site is centred on a 2 m high scarp; gas leaks at a weak to moderate rate at numerous points on either side of the scarp (Fig. 17a) and very vigorously from a limited number of points at the base of the scarp (Fig. 17b); leakage at this site does not include the diffuse style observed at the Bottaro crater. Despite the deeper water, the bubble flares from the large leakage points reach the water surface. Because only a limited number of flux measurements could be conducted, the approach and calculations made at Point 21 are more approximate than those conducted at the Bottaro crater. Here the area was mapped and filmed by the divers and the number of leakage points were counted in the immediate vicinity of the scarp and subdivided into weak (15 vents), moderate (10 vents), and strong (5 vents) flow rates based on a visual assessment. Measurements were then made on representative vents, and the value for each of the three leakage point types was multiplied by the number of such points mapped in the area. Clearly this approach assumes that the measured points are representative of the average value for each class, which is likely not the case; more extensive measurements would be needed to obtain a more precise estimate. It is also likely that the total number of weak to moderate leakage points was underestimated.

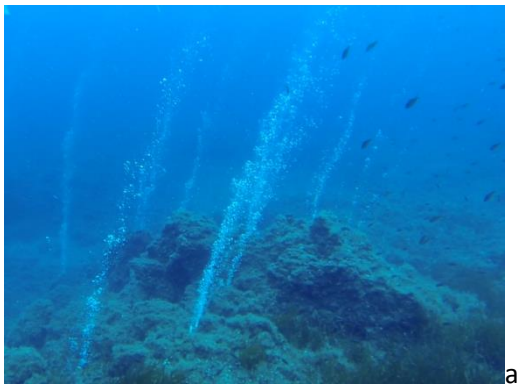
a)

b)

Fig. 17: Photographs showing the range of different flow rates at Point 21, including low to medium sized flares (a) and strong flares that traverse the 20 m water column and reach the water surface (b). Note that the darker band along the lower half of (b) is the scarp off-set of ca. 2 m.

According to these rough estimates, the total flow from the area immediately around the scarp at Point 21 is approximately twice as large as that measured for the Bottaro crater site (cf. Table 1 and 2). Gas flow is more concentrated at this site, with the occurrence of 5 very strong vents compared to the more moderate vents in Zone 3 at the Bottaro crater. To put this in perspective, the measured flux from the chosen strong vent at Point 21 (which may not have been the strongest) was more than 4 times larger than the largest at Bottaro crater (i.e. 1.3 vs 0.3 L_{STP} CO_2 / s, respectively). This strong focussed flow resulted in all 5 major vents having bubble flares that reached the water surface.

Table 2: Estimates of CO_2 leakage rates for the three vent types at the Point 21 site, given as both volume and mass flows.

	L_{STP} CO_2 / second	T CO_2 / year	% total
Weak flow vents	0.4	25	3.1
Moderate flow vents	7	403	50.1
High flow vents	5	374	46.5
Total flux	12.4	804	

During cruise POS469 (Linke, 2014) different approaches were used to assess gas fluxes. Three areas with different release rates of free gas bubbles emanating from the seafloor were selected and sampled by using ROV PHOCA.

To quantitatively assess gas fluxes and to qualitatively investigate bubble rise behavior a Bubble Box was developed and deployed at four dives at various gas seepage sites. The images grabbed from B-Box video recording show good quality with hardly any motion blur of the bubbles. Discrete gas flux measurements revealed fluxes around 330 ml per minute at 60m depth and serve as a base to cross-check later video bubble size analyses (Fig. 18). Considering the known ground base dimension of the bubble box frame of 0.2 m² and a measured integrated flux after computational “bubble trajectory” will allow for true flux assessments. By near range sonar measurements (Fig. 14) this flux will be spatially extrapolated to obtain a total flux value for one entire seep. To constrain potential bubble plume and upwelling effects a dye was injected at the base of the B-box (Fig. 18). First analyses of the videos indicate significant upwelling of the water surrounding the gas bubbles. Further evaluation of the data will finally allow to quantitatively assess gas bubble sizes, rise velocities, seep characteristica and finally fluxes.

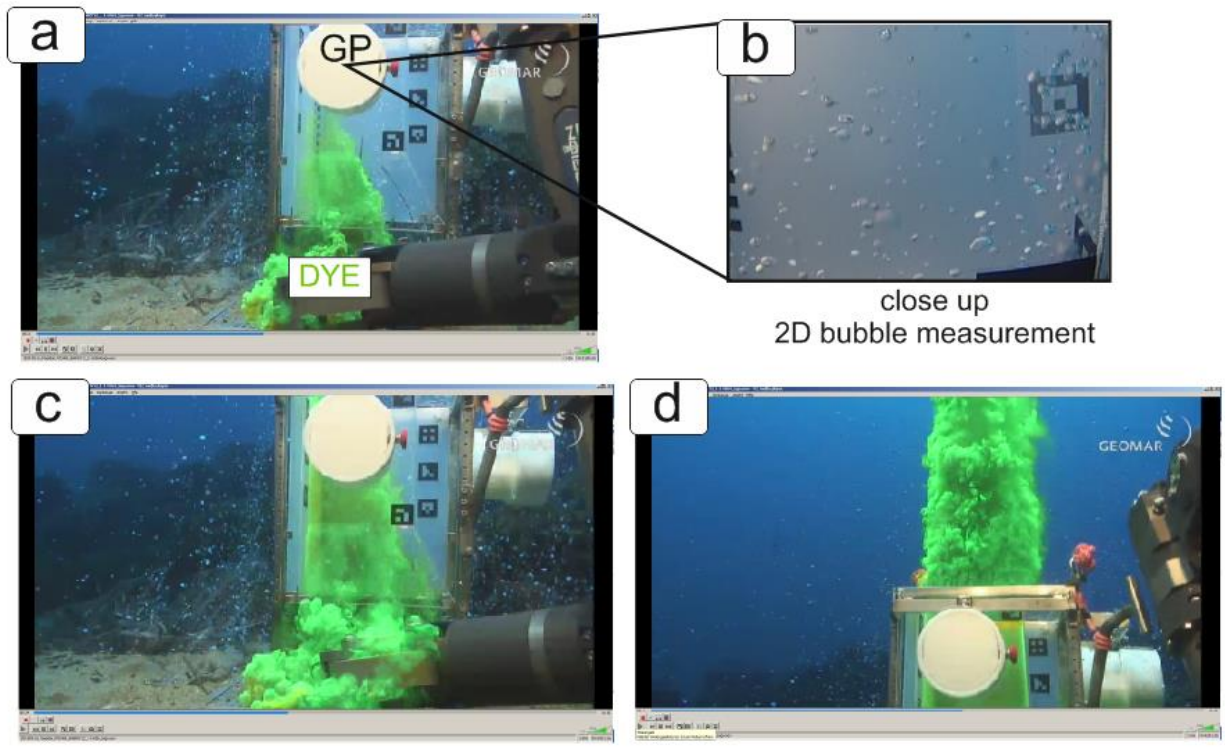

Fig. 18: Deployment of B-box at 60 m water depth showing (a) ROV camera observation of initial dye release (b) pictures taken by the GoPro (GP) camera with backlid illuminated gas bubbles within the bubble box. Squares in lower left corner are 1 cm, large squares on the right 4 cm. (c) ROV camera observation of tracer experiment shortly after (a) and a few seconds later (d) showing the vertical evolution of a gas bubble plume.

The gas sampling during POS469 was performed by placing an open (water filled) stainless steel cylinder (volume: ~ 1 L) with its funnel-shaped inlet over a bubble stream (Schmidt et al., subm.). The 1 inch ball valve of the inlet was closed after about 8 minutes when the cylinder has been totally filled with gas. The gas of the pressurized (~5 bar) cylinder was transferred onboard into pre-evacuated glass vials with pressures of 1050 mbar for subsequent measurements. The gas composition was determined onboard by gas chromatography (Shimadzu 2014, Heat Capacity Detector, He-carrier gas, packed column).

Moderate gas bubbling has been observed in the sampling area PCTD3 during ROV and Video-CTD operations at the seafloor (Schmidt et al., subm.). Usually single gas bubble streams were emanating from a smooth hard ground covered with some detrital sandy sediment, small gravels, and patches of sea grass. A few small spots were found with cm-sized vent edifices surrounded by white patches. These bacterial mats and patches of disseminated sulfur have been observed before by other authors in the overall area (e.g. Gugliandolo et al., 2006).

The frequency of bubble streams (determined within 2 x 2 m^2 patches) observed only during the deepest CTD-track in bottom view-mode (1-2 m above ground; Fig. 19), is plotted in figure 20.

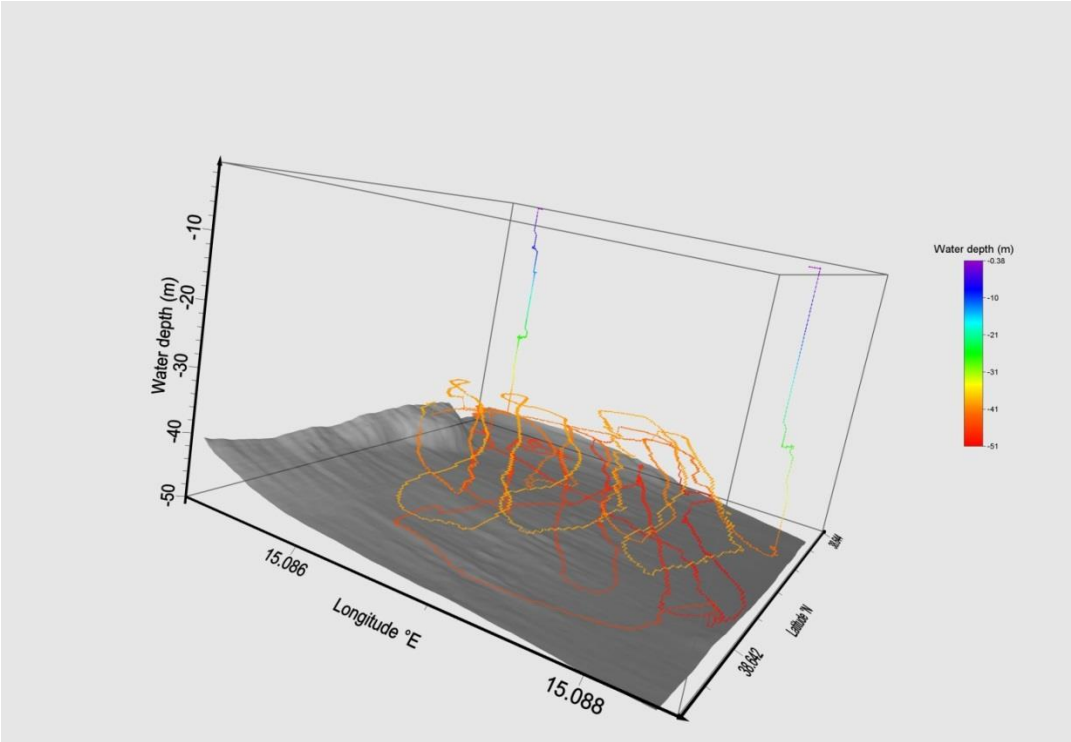

Fig. 19: 3-dimensional visualization of CTD track PCTD3 shown in figure 23. Bathymetric data of Anzidei (1998) is shown in gray shades (Schmidt et al., subm.)

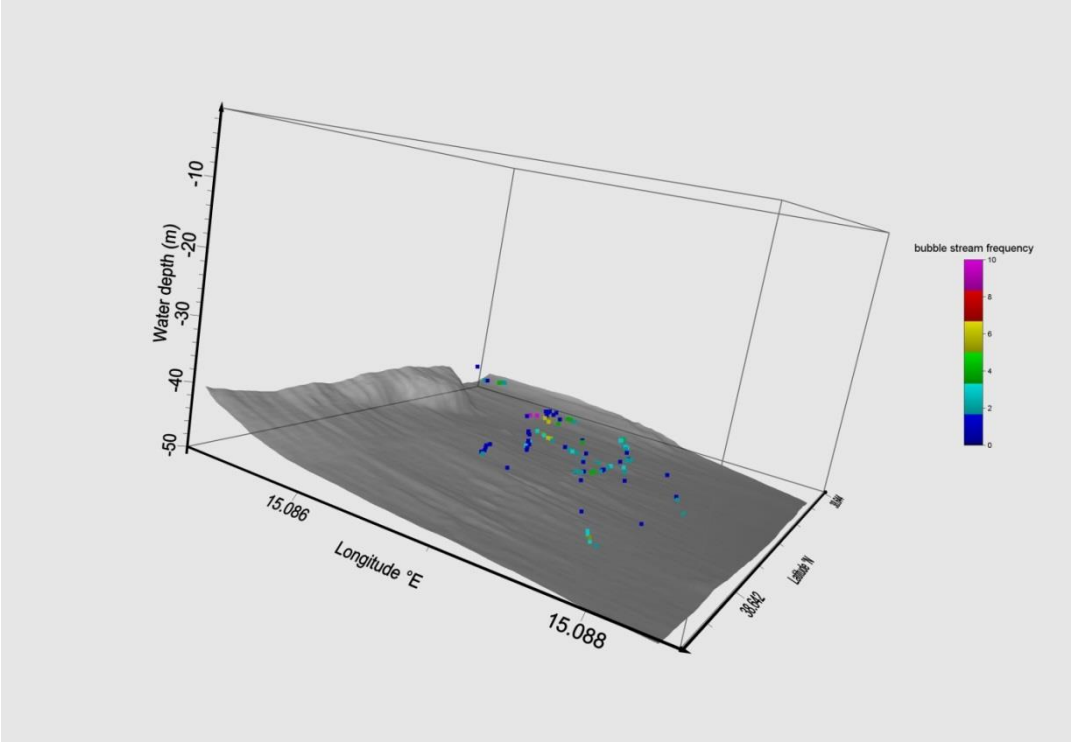

Fig. 20: Visual characterization of observed gas vents (bubble streams at the seafloor) during CTD track PCTD3 shown in figure 18. Intensity of venting is characterized by the frequency of bubble streams per video footage (~2 x 2 m^2).

Most bubble stream events (294 in total) are lined up along a NW-SE trend. This is a general direction of sub-seafloor fractures identified after the major gas eruption in 2002 (e.g. Anzidei et al., 2005) and bubble migration is probably associated to these fractures (Esposito et al., 2006).

Assuming that most of the bubble streams have been counted for the 300 x 400 m^2 sampling area one can calculate the CO_2 flux into the bottom water. An average bubble flow of 1 L per 8 min (5 bar; 95% CO_2) is used to calculate a flux of about 4 tons CO_2 per day and square kilometer (Schmidt et al., subm.)

2.3.3 Geochemical flux measurements

Building on experience and development work in previous EC-funded research projects (e.g. CO_2ReMoVe, RISCS), UniRoma has continued to improve its small, low-power consuming, low-cost, pCO_2 monitoring probes ("GasPro") within ECO_2. The goal of this development has always been to minimize costs, unit size, and power consumption so that multiple units can be deployed simultaneously, thus providing both temporal and spatial data. To this end, 20 GasPro sensors were deployed along a 20 m long, 6 m high water column transect just to the SE of the Bottaro crater (Fig. 15a) to monitor the dispersion of dissolved CO_2 (Fig. 21a).

The transect was oriented ENE-WSW, perpendicular to the long axis of the crater and the main local current direction. Five lines with four probes each were held vertically in the water column using heavy ballast and 5 L sub-surface buoys (Fig. 21b). The probes were mounted with membranes facing upwards to prevent direct contact with bubbles. The top probe on each line was positioned 2 m below the water surface, while the membrane of the bottom probes were about 50 cm above the sediment surface. The only probe with a pressure sensor was placed at the bottom of line 5. All sensors were programmed for one analysis every 10 minutes with a warm up time of 2 minutes. The total deployment period was about 2.5 days (May 27 – 30, 2013).

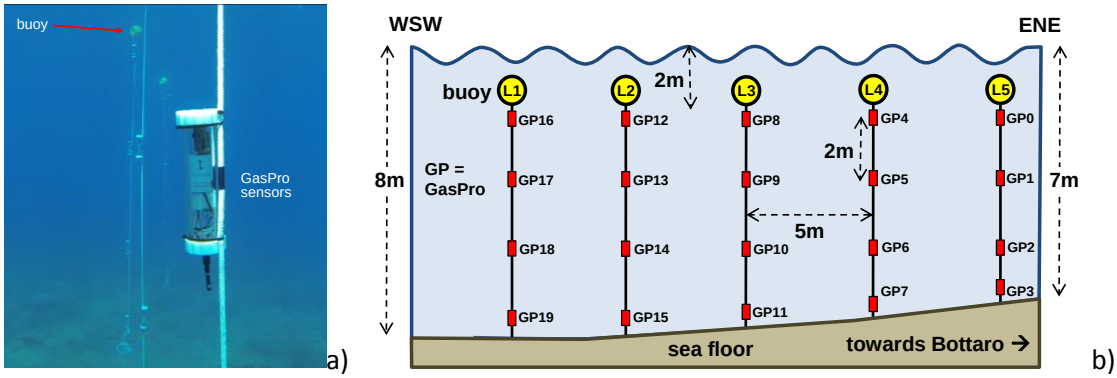

Fig. 21: Photograph (a) and schematic diagram (b) of the GasPro sensor transect deployed near the Bottaro crater.

The entire temperature and pCO_2 datasets for all 20 probes were contoured for each measurement event, resulting in 368 frames like the two shown in figure 22. All frames were animated together to show the 2D evolution of the monitored parameters over a 60 hour period. The results of this experiment, together with the video as a web-based supporting information file, have been submitted for possible publication (Graziani et al., 2014).

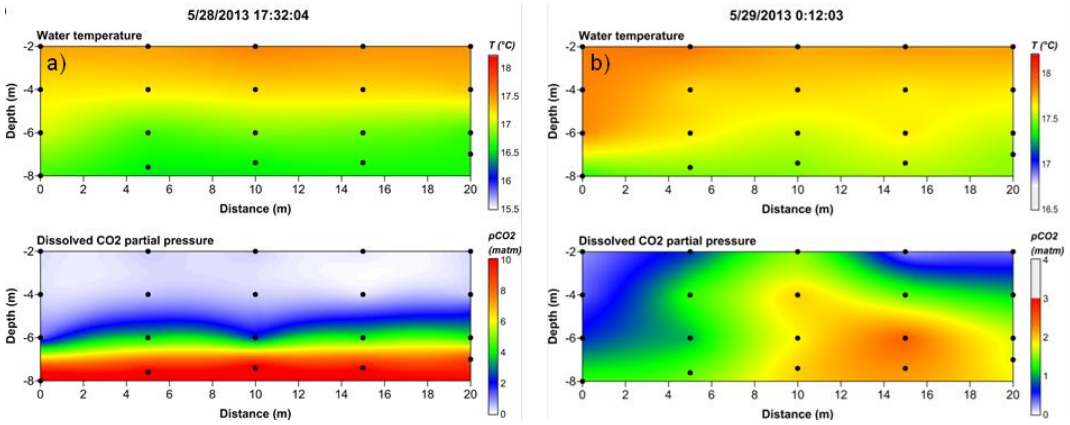

Fig. 22: Spatial distribution of temperature (top) and pCO_2 (bottom) data along the transect: development in bottom waters during a) stratified conditions and b) non-stratified conditions, where dissolved CO_2 migrates towards the sea surface. Note the different colour scales.

Results were dominated by strong anomalies that entered into the transect area via cold, bottom-water currents during stratified conditions (e.g. Fig. 22a), with maximum values exceeding 10 matm in the probes closest to the sediments. These anomalies often entered from one side of the transect, then proceeded to fluctuate back and forth across it before exiting to one side or dissipating. The association with colder waters (1 to 2.5°C lower) and the duration of some of these events up to 2-3 hours implies that these anomalies originate in deeper waters where other CO_2 leaks occur and that this water is forced up onto the platform via upwelling currents. Smaller anomalies, often occurring higher up in the water column and not in association with colder waters may have a more local origin linked to leakage from the Bottaro crater area itself. Unfortunately, the lack of current data does not allow us to make a more definitive interpretation of the origin of the anomalies and does not permit us to convert these concentration values into an estimate of the total dissolved CO_2 flux across the 2D section. Whereas many of the pCO_2 anomalies were restricted to the bottom waters, a number of smaller events were observed to move towards the water surface during less stratified conditions (Fig. 22b; note different colour scale). In these cases mixing processes, some induced by the initial entrance of the upwelling events themselves, force deeper waters upwards where the leaking CO_2 can be released to the atmosphere.

During RV Poseidon cruise POS469 (Linke, 2014) 4 hydrocast stations and 7 pump-CTD tracks were performed in the area off Panarea (Fig. 23). The distribution of pCO_2 in the near field of submarine volcanic gas flares in shallow water depths between 40 – 80 m below sea level was continuously monitored using three different and independent methodologies. In situ Non Dispersive Infrared (NDIR) spectrometry, pH measurements, and onboard Membrane Inlet Mass Spectrometry (MIMS) were used to determine the fate of rising CO_2 bubbles and the dissolved CO_2 plume patterns in defined working areas with different gas discharge rates (areas Pump-CTD 3-7 in Fig. 23).

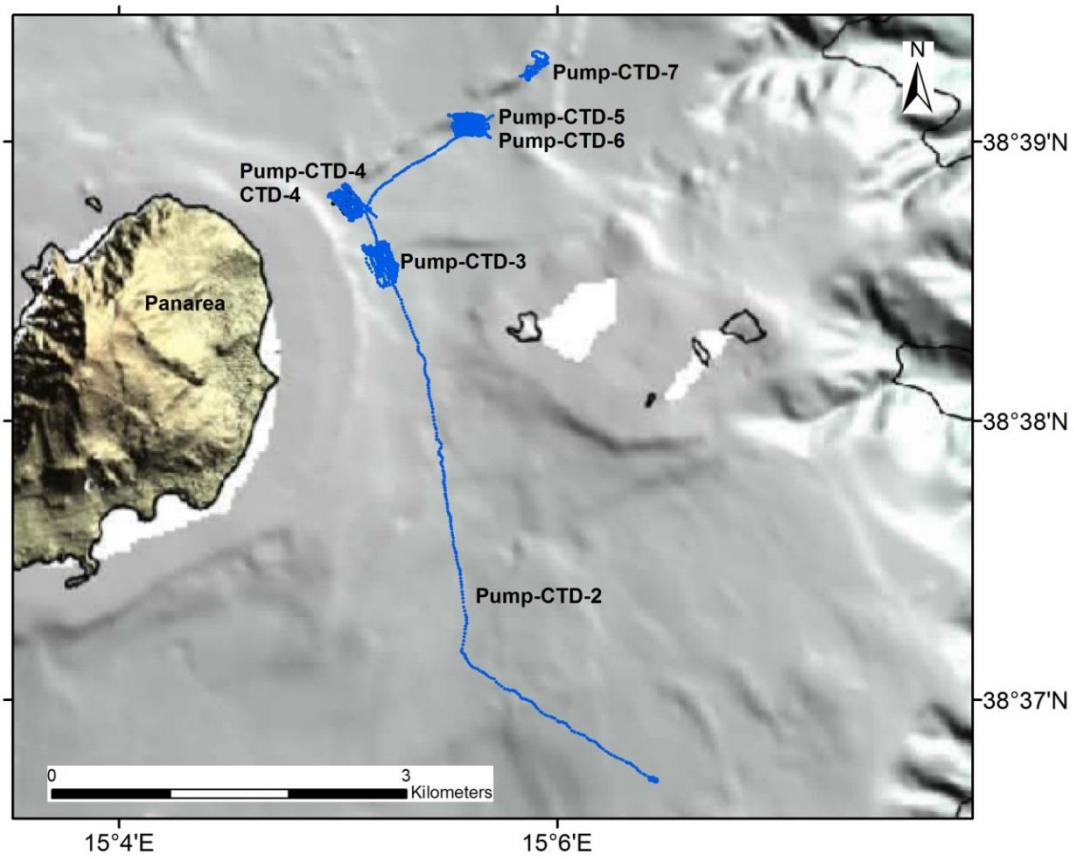

Fig. 23: Bathymetric map of Panarea (Chiocci et al., 2013) with marked (blue lines) CTD tracks.

The in situ sensor carrier platform, a towed video-controlled water sampling rosette, equipped with CTD, guaranteed excellent ground truthing of seafloor characteristics and bubble discharge (Linke et al., subm.). Sensor data and near seafloor observations indicated that the gas bubbles (<9 mm in diameter; >97% Vol. of CO_2) from the first working area in depths up to 50 m below sea level dissolved very rapidly within the first 10 m above seafloor (Fig. 24).

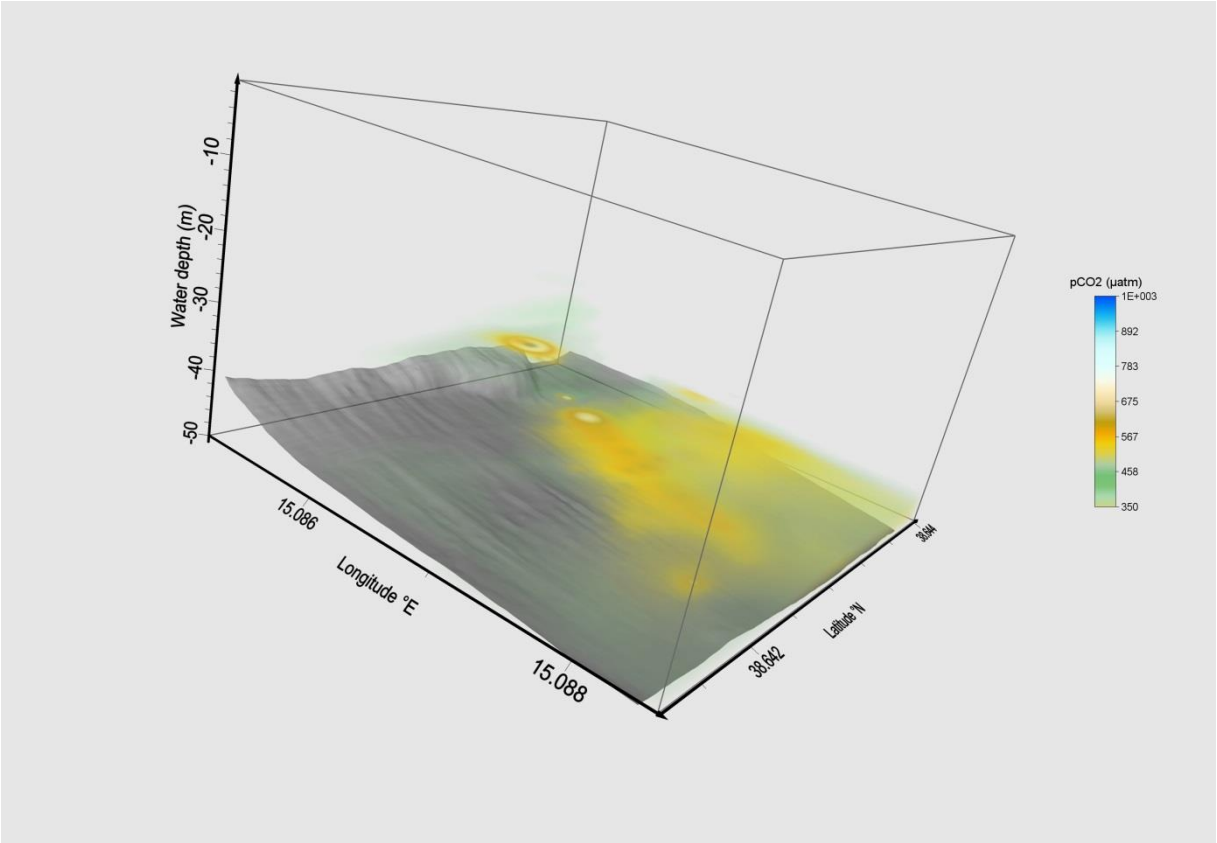

Fig. 24: Volume-rendered pCO_2-data (HydroC^{TM} sensor) during CTD track PCTD3 showing strongest dissolved CO_2 accumulation closest to the seafloor (Schmidt et al., subm.)

Bottom water masses enriched with pCO_2 (up to 1100 µatm) showed low pH values (up to 7.80) and tended to spread rather down-slope west than following the actual weak current in SSE-SSW direction (Schmidt et al., subm.)

2.3.4 Impact of CO_2 and other geochemical species on biological communities

During the ECO2 project, Scientists of MPI (Germany), HYDRA (Italy), UGent (Belgium), GEOMAR (Germany), OGS (Italy) and UniRoma (Italy) have studied natural CO_2 vents as analogues for the long-term impact of CO_2 leakage on shallow water and continental margin ecosystems, communities, species and their function. Several sites were sampled close to Basiluzzo islet and Panarea Island as reported in the deliverable 4.1.

In June 2012 and May 2014, during joint campaigns with WP4 and WP3, OGS and UniRoma1 collected water samples for chemical and biological analyses along a transect, crossing a venting area between Bottaro and Lisca Bianca Isles (LB transect, see Fig. 15a). This area is close to the "Bottaro crater", where gas flux from the sea floor to the overlying water column were measured and the spread of dissolved CO_2 was monitored. In this area, gas emissions characterized by the smell of H_2S were also detected. CTD data defining water column stratification and pH distribution were used to decide the location and depth of discrete water sampling (collected at 7 stations) for various chemical and biological analyses. Selected parameters are plotted together to summarize the results (from June 2012 campaign) and to better highlight potential associations and impacts linked to the leaking CO_2.

The temperature and density anomaly data along the LB transect (Fig. 25a) showed warmer and low density water which starts from the bottom of station LB3 and spreads to the surface of stations LB1, LB2, and LB3. In correspondence with these geothermal spring waters the hydrogen sulphide concentrations (Fig. 25d) and the partial pressure of CO_2 (max = 11020 µatm, Fig. 25b) exhibited very high values. These results clearly show the presence of gas leakage from the seabed which can influence the water column chemistry. In particular, the same water mass was strongly acidified (pHT min = 6.680, Fig. 25c) in association with aragonite undersaturation levels (ΩAr < 1, Fig. 25e). Such extreme seawater acidity represents a typical condition of the CO_2 vents in this area and it could easily lead to the dissolution of calcareous shells or skeletons of calcifying organisms. Silicate concentrations were also observed to increase significantly in correspondence with the hydrothermal vents (Fig. 25f), probably as a consequence of the turbulence induced by the seepage of gas bubbles which transport upwards the interstitial water enriched in silicates. Despite the occurrence of this significant leakage-related trend, the other measured nutrients do not show corresponding increases with the venting phenomena (i.e. ammonium and phosphate might be expected to increase together with the silicates). The reason of this discrepancy is under investigation.

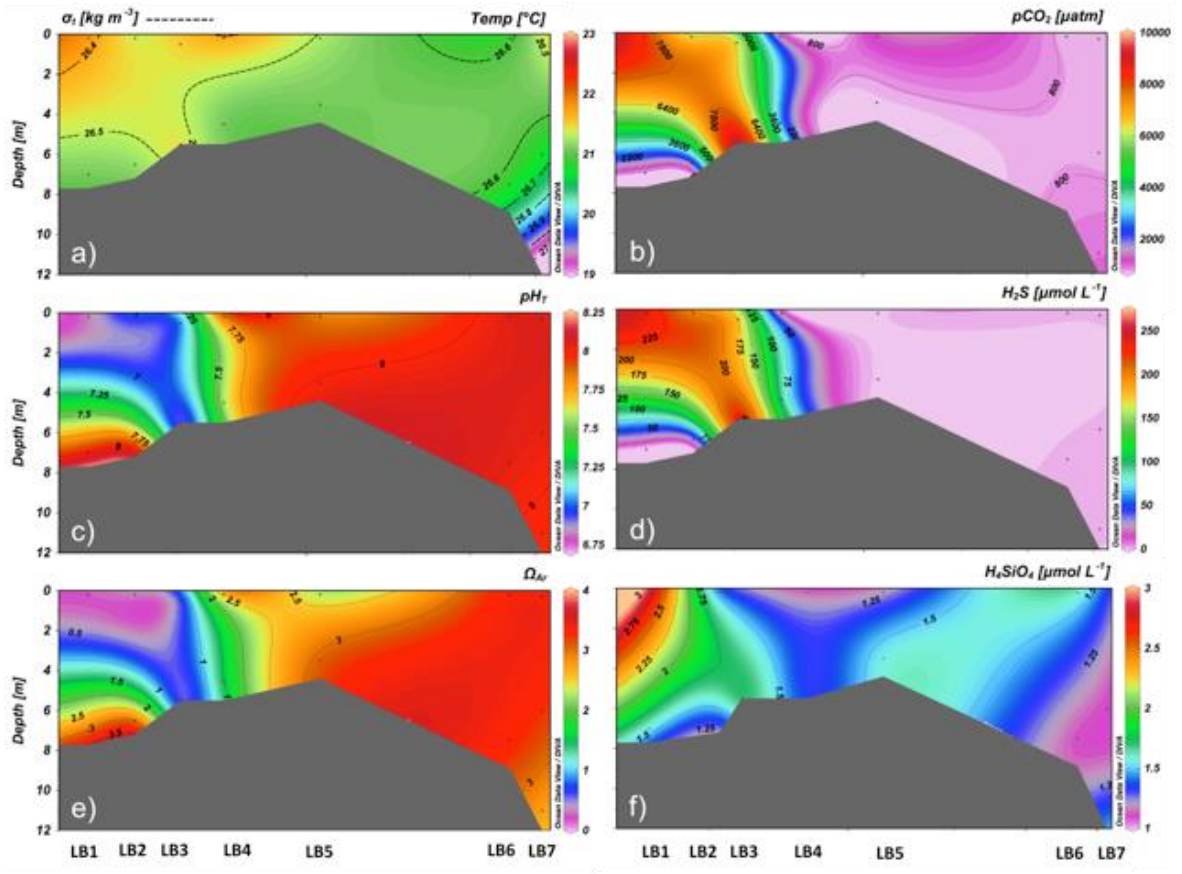

Fig. 25: Contour plot of (a) temperature - density anomaly (σt – dashed isolines), (b) partial pressure of CO_2 (pCO_2), (c) pH at total scale (pHT), (d) hydrogen sulphide, (e) aragonite saturation state (ΩAr), and (f) silicic acid, along the LB transect between Bottaro and Lisca Bianca Islets.

Microzooplankton was analysed synoptically with phytoplankton. The impact of CO_2 on the abundance and diversity of both communities was investigated to increase our capability to predict marine ecosystem response to potential CO_2 leakage. Contrarily to the observation during the PaCO2

/ ECO2 cruise (July/August 2011, McGinnis et al. 2012), where the heterotrophic prokaryotes (HP) were stimulated by gas leakage in the proximity of the vents in mobilisation processes, the campaign conducted in June 2012 along the LB transect revealed a negative impact of gas emissions both in terms of heterotrophic abundance and activity. This could be due to the presence of H_2S in these vents. However, no particular differences were identified (both amongst the stations and the sampled depths) for the phytoplankton community in terms of either abundances or biodiversity.

From these preliminary results, natural CO_2 emissions in this area do not seem to have any clear influence on the phytoplankton and microzooplankton communities and the differences noted seem to be linked mainly to seasonal variations rather than CO_2 emissions. This may be due, in part, to the strong and complex currents in the area that guarantee lateral transport of the monitored species in the water column as well as efficient mixing of CO_2.

2.4 Salt Dome Juist

During a pre-site mapping study in October 2008 (Alkor cruise AL328), an area with strong acoustic flares was discovered at a shallow (~30 m) study site above a salt dome structure in the Southern German North Sea about 30 km offshore the East-Frisian Island Juist. Shallow seismic investigations indicate Quaternary sediment structures i.e. valleys and depressions which are probably filled with organic-rich deposits (e.g. peats and lignites). Decomposition of the organic matter led to the accumulation of shallow gas (Streif, 2002). Furthermore, deep seismic exploration in this area has revealed a complex structure of salt diapirism, tectonic faults, bright spots, and several kilometres deep gas/fluid migration patterns reaching the seafloor in certain areas.

During the first study, CO_2 values ranging from ~10-20 times above background, and a peak CO_2 value >53 times higher than background were measured, indicating a possible CO_2 point source from the seafloor. Measured pH values of around 6.8 supported modelled pH values for the observed high CO_2 concentration (McGinnis et al., 2011b). While isotope signatures pointed to a biogenic source, the origin remained inconclusive because of dilution.

During a follow-up cruise in 2009 (CE0913) this area was revisited with a ROV and a prototype of a video-guided water sampling rosette carrying enhanced sensors and an immersion pump that continuously pumped bottom water into the laboratory, where it was connected to a Membrane Inlet Mass Spectrometer (Linke et al., 2010). Despite the efforts, the results remained inconclusive as no repetition of the former measurements was possible. However, pH in surface sediments dropped down to about 5, probably indicating both, transport of dissolved CO_2 from a deeper source and respiration. Nevertheless, this site was chosen as a potential natural analogue to study the effects of carbon sequestration below the seafloor. Within ECO2, 2 cruises (AL374 and HE377) were conducted to revisit the Salt Dome Juist site.

2.4.1 Hydro-acoustic measurements

During cruise AL374 towed CTD tracks at Salt Dome Juist (stations CTD01 and -03) were performed on the 30th of May, 2011 at a water depth of about 29 m (Linke et al., 2011). Acoustic scatterers were observed early in the morning during the first part of CTD01-2 by the ships own Simrad 38 kHz echosounder (Fig. 26). Due to the shape of the acoustic signal it seems likely that they have to be attributed to fish instead of gas bubbles. Note that no acoustic signals were recorded after 6 am on the 30th for the next 24 hours in the working area “Salt Dome Juist”.

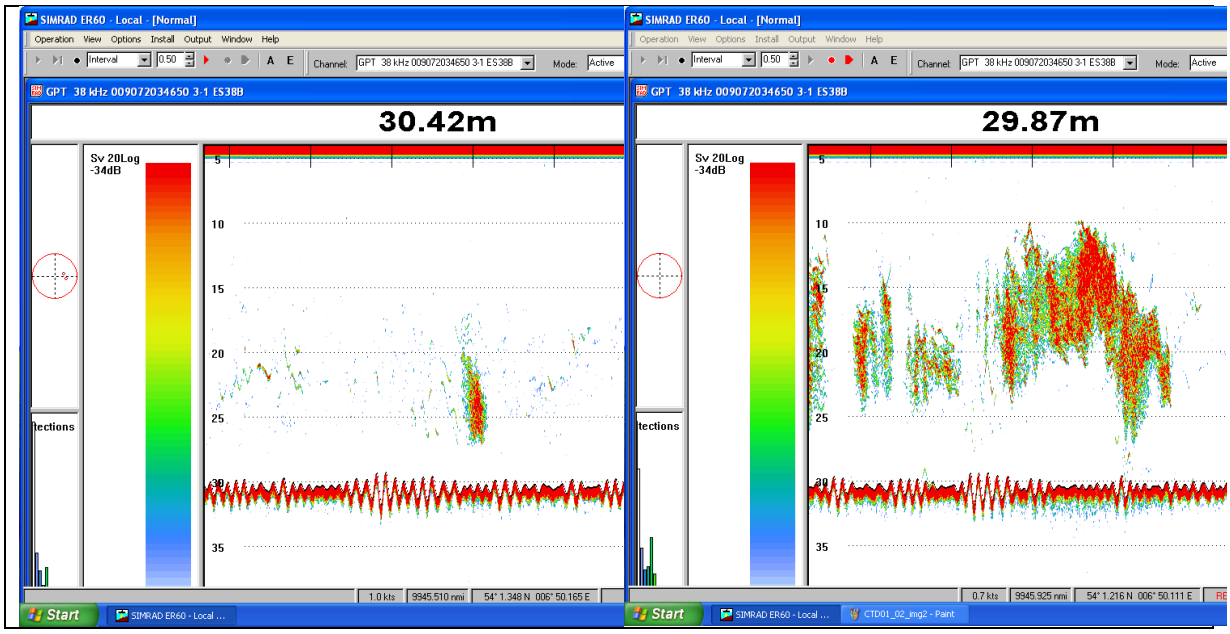

Fig. 26: Acoustic scatterers recorded with the 38 kHz echosounder during Alkor 374 cruise at Salt Dome Juist (CTD01-2).

During cruise HE377 only weak seepage activity (Fig. 27) was visible during the mapping activities (Wenzhöfer et al., 2012).

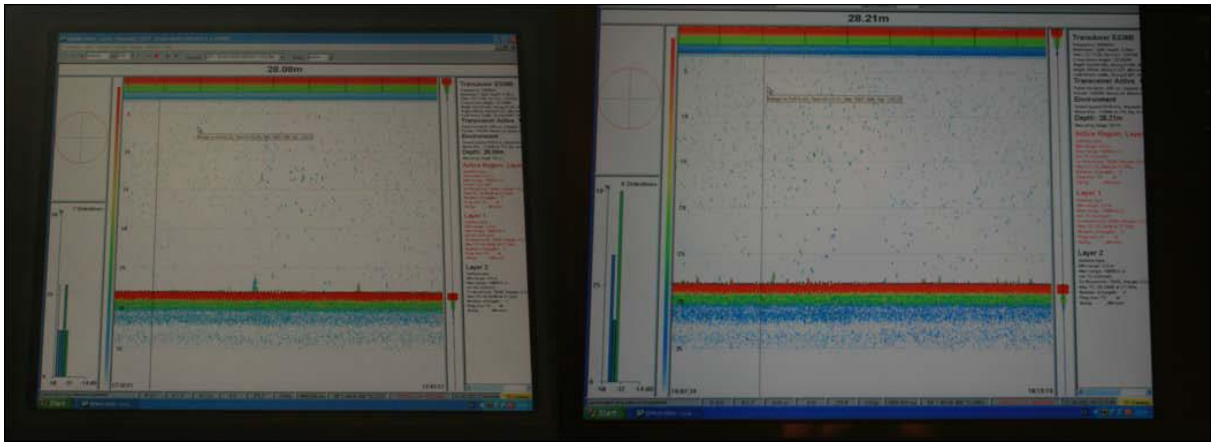

Fig. 27: Weak gas flares recorded with the 38 kHz echosounder during Heincke 377 cruise at Salt Dome Juist.

2.4.2 Gas fluxes in the water column

Despite many deployments of video-guided instrumentation (OFOS, ROV), none of the ground truthing techniques was able to find active gas bubble emissions from the seafloor. Therefore, gas flux measurements could not be performed.

2.4.3 Geochemical flux measurements

During cruise AL374 the CO_2-concentrations determined by the Contros HydroC sensor during the near-seafloor tracks (at about 29 mbsl) were constant at about 335 ppm CH_4. However, the CO_2-concentrations changed from 335 to 345 ppm during slack water (Fig. 28; CTD03 track). Methane concentrations in Niskin water samples, determined by gas chromatography, ranged between 1.6

and 2.4 nM. No CH_4 concentration changes were measured by HydroC-CH_4 in the Salt Dome Juist area (detection limit ~200 nM).

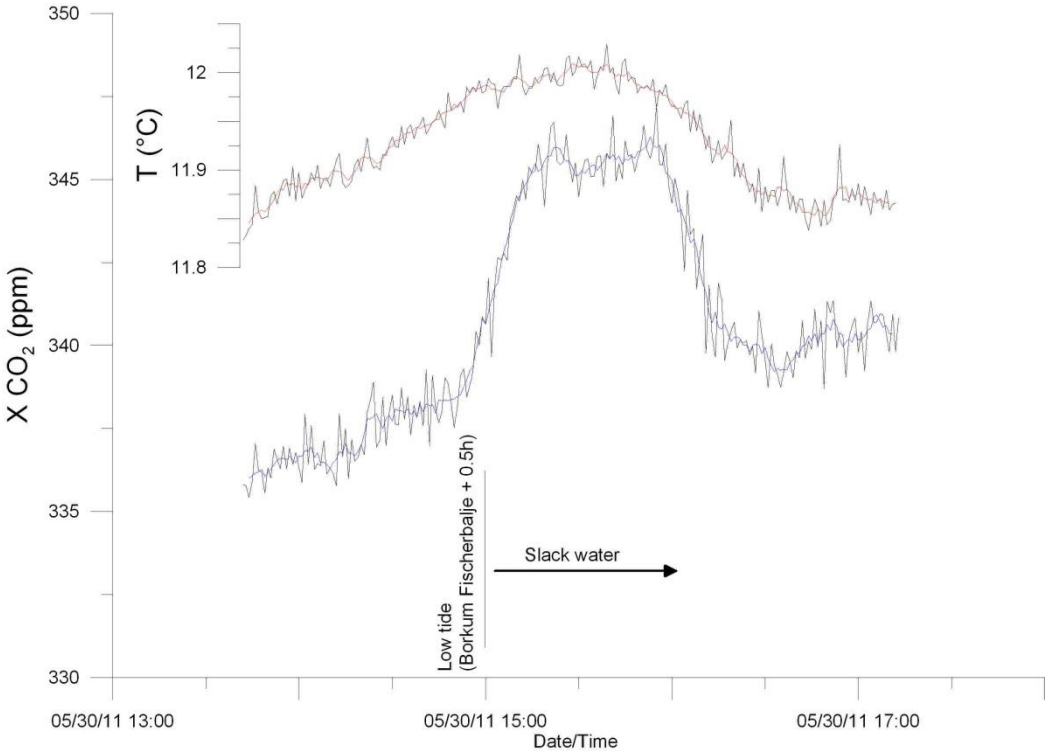

Fig. 28: Temperature and CO_2 concentration change during CTD03-track at 29 mbsl (slack water time is indicated).

During cruise HE377, the AUV of the Alfred Wegener Institute (AWI, Fig. 29) was used to perform extensive search grids closely above the seafloor to detect CO_2 anomalies (Wenzhöfer et al., 2012). The vehicle was equipped with a Contros CO_2 sensor and CO_2 microelectrodes (Bedford, New Hampshire). The microelectrodes were mounted on the so-called BioGeoChemical (BGC) Module, which was developed at the Max Planck Institute for Marine Microbiology (MPI) in Bremen.

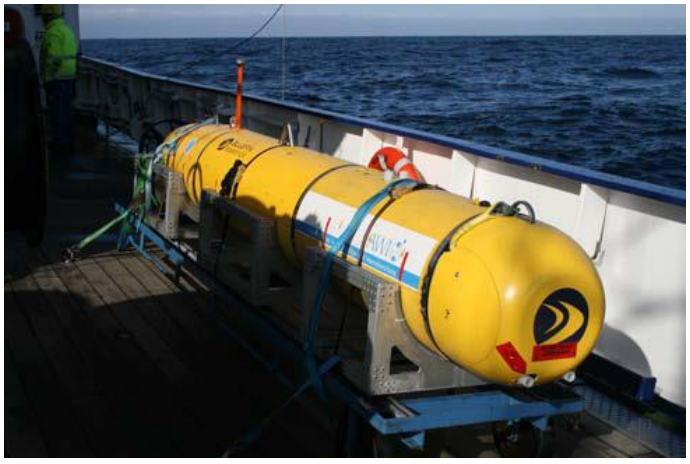

Fig. 29: AUV (AWI) for water column studies above the seafloor.

In total, the AUV accomplished three dives during HE-377. Submerged, the vehicle covered a distance of 68 km and investigated an area of 2.5 km² with a spatial resolution of 60 m. North of the island of Juist, it was possible to trim and test the vehicle (Dive 1) and to accomplish two search grids (Dive 2 + 3). The search grids of both dives overlapped a little to ensure a gapless investigation of the area. The search grids of the dives 2 (22.04.12) and 3 (23.04.12) can be seen in figure 30. During both dives the vehicle kept a distance of 5 m to the seafloor and moved at a speed of 1.5 m/s.

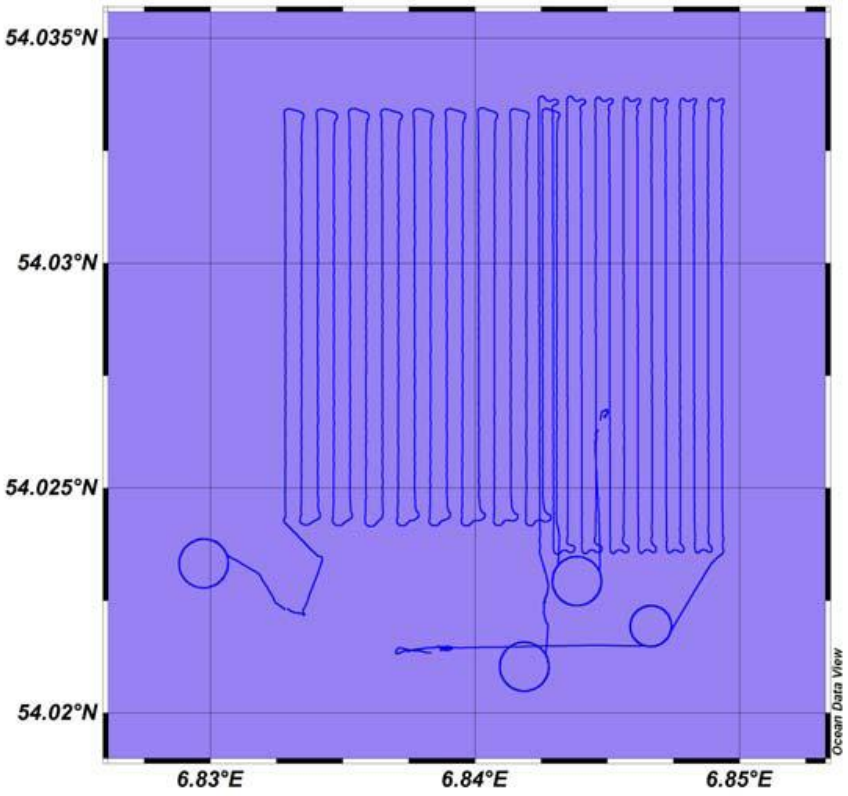

Fig. 30: AUV search grids during HE337.

Figure 31 shows the monitored water column CO_2 value 5 m above seafloor in the investigated area graphically. The CO_2 map reveals that the CO_2 value was generally higher during the third dive but no gradients could be detected. In contrast, a smooth gradient of 2 µatm in the CO_2 partial pressure could be observed a day before (Dive 2; 22.04.12). As this gradient was very small and apparently parallel to the tracks of the search grid, it was most likely caused by tidal effects. Thus it rather was a "temporal" than a "spatial" gradient and it could not be traced back to gas seeps on the sea floor.

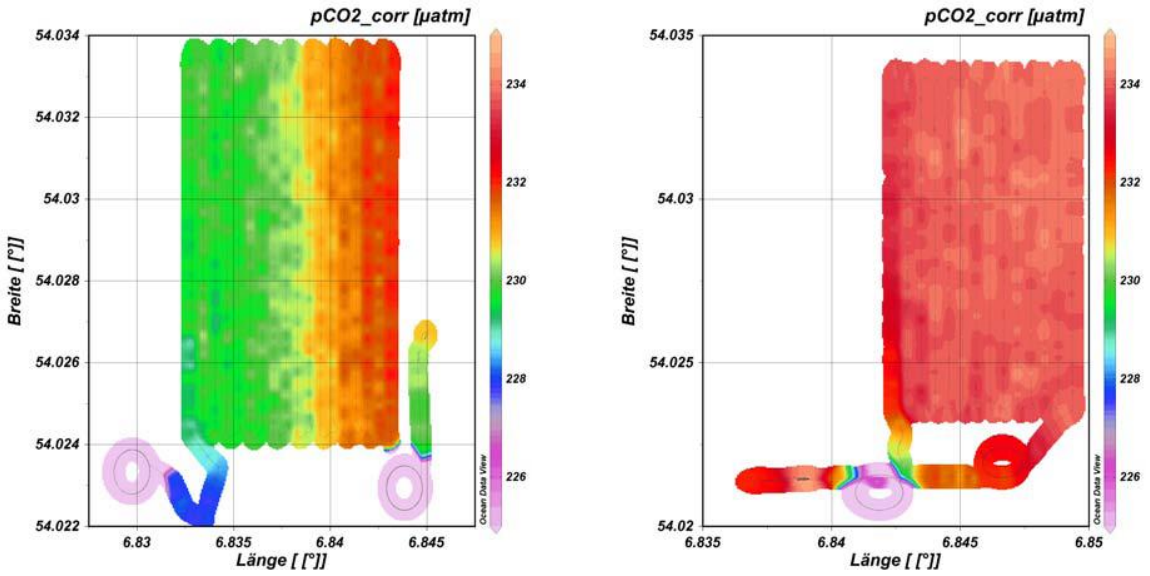

Fig. 31: a) CO_2 distribution during Dive 2 (22.04.12) and b) CO_2 distribution during Dive 3 (23.04.12).

Although the sonar of RV Heincke was able to detect weak gas flares, the AUV bound measurements did not show point-shaped CO_2 sources. It is possible that the response time of currently available CO_2 sensors are too long to clearly detect such small sources with a relatively fast moving platform like an AUV.

On the other hand the distance of the vehicle to the sea floor plays a key role. The vehicle´s sensors can only detect dissolved substances. The closer the vehicle comes to the sea floor the less time is available for the gas bubbles to dissolve in the water. At the same time, as water currents push the bubbles around, a relatively small distance between the vehicle and the sea floor is an important precondition to exactly detect the location of the gas seeps. By keeping a greater distance from the sea floor the possibility to find seepage will increase. However the information of where to find the source of the gas gets lost. In this respect, the right distance from the sea floor during these missions will remain a compromise between “as close as possible, as far as necessary” (Wenzhöfer et al., 2012).

The in situ flux studies using benthic lander systems (Benthic Chamber Lander with 3 chambers and one microprofiler as well as an Eddy-lander) failed during cruise HE377 because we lost our lander during the recovery of the first deployment (Wenzhöfer et al., 2012). The in situ studies were intended to determine benthic exchange rates, fluid/gas fluxes and to measure high-resolution microprofiles. With intensive dredging during the nights we were able to retrieve our lander back but only at the end of the expedition thus no further deployments were possible during HE377.

2.4.4 Impact of CO_2 and other geochemical species on biological communities

To test the sensitivity of sandy infauna bivalve communities to CO_2 stress, a 3 month long experiment using communities from the Western Baltic Sea (11/2011-03/2012) has been carried out. Using 6 treatments (control – 20,000 µatm) with 6 replicates each, the three most abundant bivalve species (*Cerastoderma edule*, *Mya arenaria*, *Macoma balthica*) and associated sediment bacterial and meiofauna communities were incubated for 3 months. These species were chosen, as some of them live in the sediments of the North Sea as well. Communities were fed continuously with fixed

amounts of cultured algae and samples were taken to assess bivalve growth, calcification and condition, microbial diversity and meiofauna composition (Morgan et al. 2014). Results indicate higher bivalve mortality coupled to intensive shell dissolution, with smaller organisms demonstrating greater vulnerability (at pCO_2 values of >1,500 µatm). Interestingly, bivalves left the sediment prior to death and accumulated on the sediment surface, suggesting that cost effective video – based monitoring techniques could be feasible to identify sea floor regions exposed to (very) high seawater pCO_2.

3 Sleipner storage site

The Sleipner CO_2 storage site has been in operation since 1996 by Statoil. More than 16 million m^3 of CO_2 have been injected into a saline aquifer (Utsira sand formation) located in the Norwegian sector of the North Sea at ~80 m water depth and ~900 m sediment depth (Chatwick et al., 2004). Sleipner is by far the best-studied and most advanced offshore storage site in the world. The spread of CO_2 in the reservoir formation has been studied and monitored in detail by the operator and within other research projects using 3-D time-lapse seismic data (Arts et al., 2004; Chadwick et al., 2009). Within the ECO_2 project, an intense field program was conducted to study the fluxes across the seabed which included measurements at abandoned wells and the newly discovered "Hugin" fracture (Fig. 32).

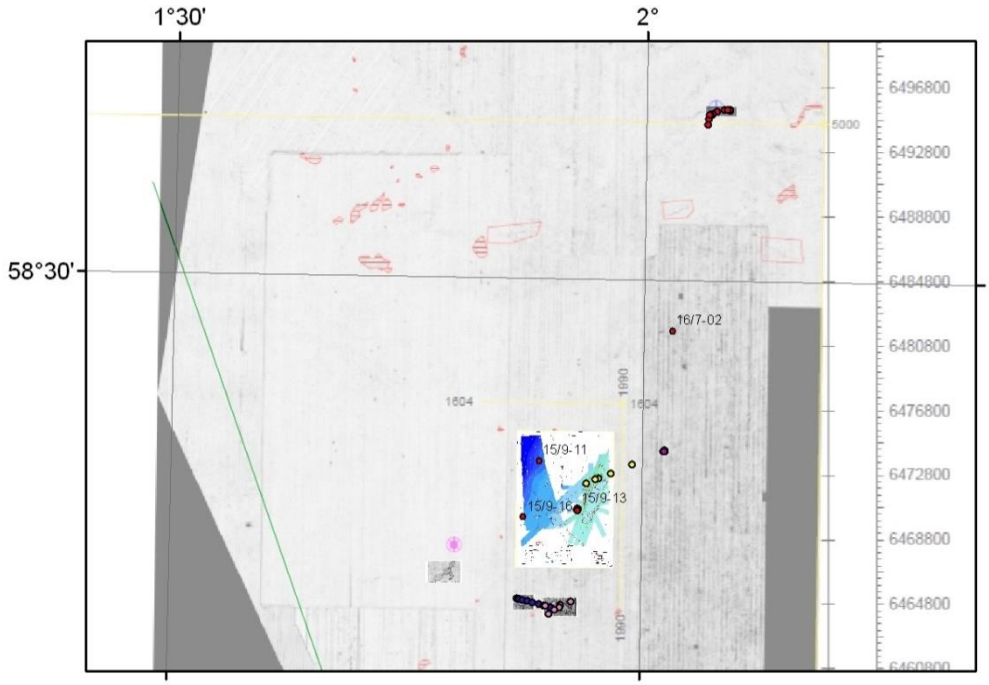

Fig. 32: Bathymetric map of the «Sleipner» area (blue color). Un-labeled colored circles mark positions of water column samples taken by Niskin bottles during cruise CE12010 (Linke, 2012). Labeled red circles mark selected abandoned wells. The gray-shaded area provides background data from seismic data evaluation (red polygones mark burried shallow gas and seismic chimney structures).

3.1 Hydro-acoustic measurements

Besides a comprehensive geochemical and benthos ecological program during the first ECO_2 research cruise AL374 with RV Alkor in May/June 2011 led by GEOMAR (Linke, 2011), sediment echo sounder (SES) and multibeam data were collected in the vicinity of the Sleipner platform. The surveyed area

covers the overburden of the CO_2 plume and several abandoned wells. The data were analyzed in the frame of a bachelor thesis for evidence of free gas in the water column and in the shallow sediments. As a first result, we were able to create a bathymetric grid, which showed manmade structures like pipelines and a supply hub north of the platform and the absence of pronounced geological features. The SES data revealed 18 anomalies in the water column that could be interpreted as gas flares (Fig. 33A). The flares cluster in an area south of the production platform and their signals could even be identified in the multibeam data (Fig. 33B). In addition, we were able to identify several randomly distributed acoustic anomalies in the shallow underground. These anomalies include bright spots as well as areas of acoustic blanking that can be related to shallow gas accumulations (Fig. 33C, D). The observed anomalies appear not to be related to the CO_2 storage; at least no direct connection could be identified. For a detailed discussion of the results we refer to the Bachelor thesis "Seafloor heterogeneities in the central North Sea: potential fluid migration pathways" by Herreilers (2012).

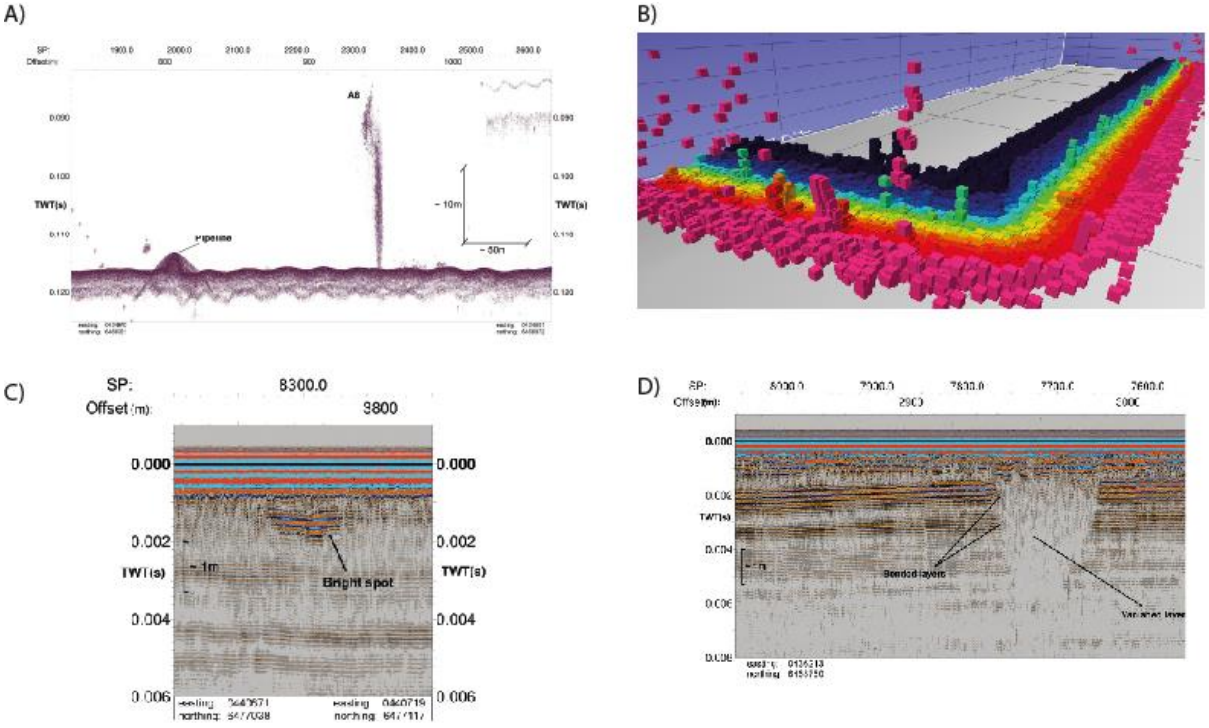

Fig. 33: A) Flare in the water column (SES); B) Water column soundings by the multibeam; C) Bright spot (SES); D) Zone of acoustic blanking (SES).

The R/V G.O. Sars revisited the Sleipner area in 2012, collecting multibeam and single-beam echosounder data. In addition to the G.O. Sars, the R/V James Cook and R/V Alkor collected multibeam and single beam data in 2013. All of the cruises collected data that is not useable for water column or multibeam mapping purposes. This was due to a variety of acquisition errors, most commonly errors in software setup, or the concurrent collection of data on systems that strongly interfere with MBES acquisition.

The presence of gas within sediments is traditionally detected using expensive, complicated and time-consuming 3D seismic techniques. During NOC cruise JC77 (Connelly, 2012), a significantly cheaper and more readily available system was tested. This involved equipping the NOC Autosub autonomous underwater vehicle (AUV) with Chirp transducers, and conducting an extensive survey of the Sleipner area and its surrounding. The data acquired, some of which is shown in figure 34, provide clear evidence of the suitability of this system for imaging gas pockets located within the top

3 m of the seabed sediments in the central North Sea. Pockets of shallow gas are clearly visible both beneath the "Hugin" fracture, and in the vicinity of an abandoned exploration well. Deeper depth penetration is possible, but is limited by power available for the AUV operations.

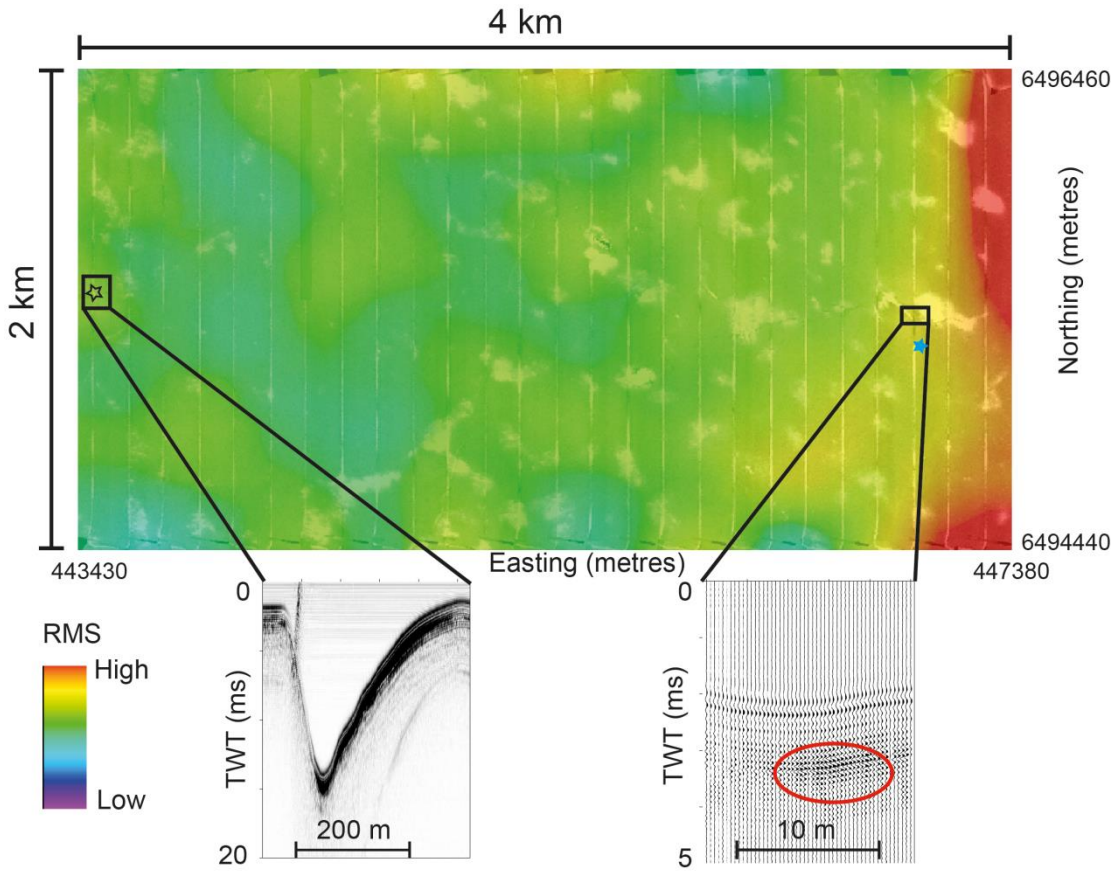

Fig. 34: Seismic images of two-way travel time (TWT) in sediments beneath an abandoned well with gas injected into the water column (left-hand side) and the Hugin fracture (right hand side), about 20 km north of the Sleipner storage site. Darker regions indicate the presence of gas. (RMS= Root Mean Square amplitude).

The use of shipboard multibeam echo sounders for detecting leakage through the imaging of bubbles as they pass from the sediment into the water column is well reported and has been used to locate leaking wells in the North Sea and other areas. Great efforts are being made to use these systems to quantify the gas fluxes into the water column, but to date there is no clear method of converting these data into reliable fluxes. These 'active' sonar techniques can be complemented by approaches using passive systems such as the deployment of hydrophones on the seabed in the vicinity of leaking gas. Although not tested on cruise JC77, a system of passive hydrophones was deployed by the NOC in a controlled sub-seafloor CO_2 release experiment, and inversion techniques were used to quantify fluxes of CO_2 across the seafloor (Leighton and White, 2011). The calculated fluxes corresponded well with the direct measurements of CO_2 flux made by divers.

3.2 Gas fluxes in the water column

Visual observations made by using a ROV confirmed that gas bubbles were exiting the seafloor above 3 abandoned wells in the Sleipner area. To constrain the composition of these bubbles seeping through the sediments into the water column, free gas samples were collected at these wells (Fig. 35). At all 3 sampled abandoned wells, CH_4 contents of between 99.0 and 99.3 % were determined. A corresponding CH_4 carbon isotope composition of -75.5 ± 0.6 ‰ and C1/C2+C3 ratios >1000 for all investigated wells point to a biogenic carbon source of the detected CH_4.

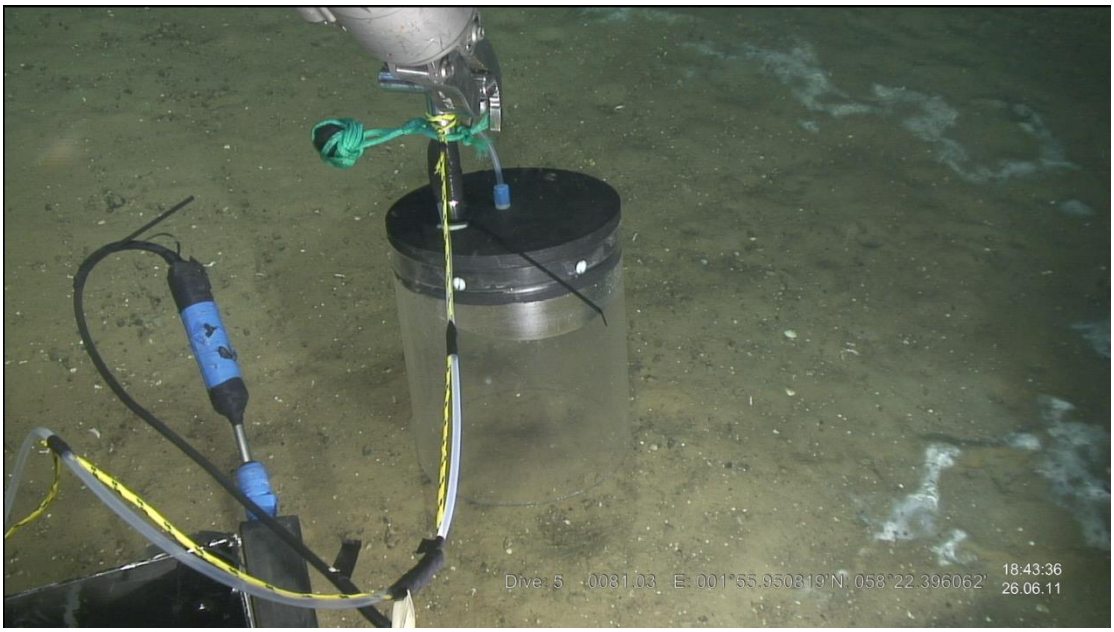

Fig. 35: Collection of gas bubbles exiting the seafloor by using a sampling cylinder that allows to determine the sampled volume over time.

To estimate the CH_4 flux rate at the sediment-seawater interface, gas bubbles were sampled in a sampling cylinder with a volume of 10.7 litres (Fig. 35) at all three investigated abandoned wells (Wells 15/9-13, 15/9-11 and 15/9-16). Thereby, the time of sampling was stopped (14 to 30 minutes depending on the sampled well) as well as the collected amount of gas during this time was about 1.5 litres for each well. This resulted in an average CH_4 flow rate of about 16 t/year per abandoned well.

Methane concentration measurements in the Sleipner water column suggest an enhanced CH_4 concentration in this area compared to a background cast obtained about 90 km NE of the Sleipner CO_2 storage site. The distribution of the dissolved CH_4 in the water column represents the prevailing water layer density pattern at the time of sampling. Thus, most of the CH_4 is accumulated at a water depth of about 50 to 60 m resulting in overall elevated CH_4 contents at these depths. Thus, the distinct density layers of the water column act as a natural barrier for the rise of CH_4 through the water column during summer.

These measurements agree very well with the GEOMAR studies, where three abandoned wells (15/9-13, 16/7-2; 16/4-2) at 81-93 m water depth in the Norwegian sector of the North Sea were investigated, all of which show gas seepage into the bottom water (Fig. 36). The seep gas at the wells consists mainly of methane (85-89 Vol.%) that originates from shallow gas pockets in the sedimentary overburden above the gas reservoirs that the wells were drilled into. This is in

agreement with high amplitude anomalies in the seismic data (i.e. bright spots and zones with chaotic signatures) indicating the evidence of gas in 600-750 m below the seafloor. The composition of the emanated gas, i.e. C_1/C_{2+} ratio larger than 1000, and $\delta^{13}C$ values of CH_4 lighter than-70 ‰ VPDB clearly points towards a biogenic origin (Vielstädte et al., submitted 2014).

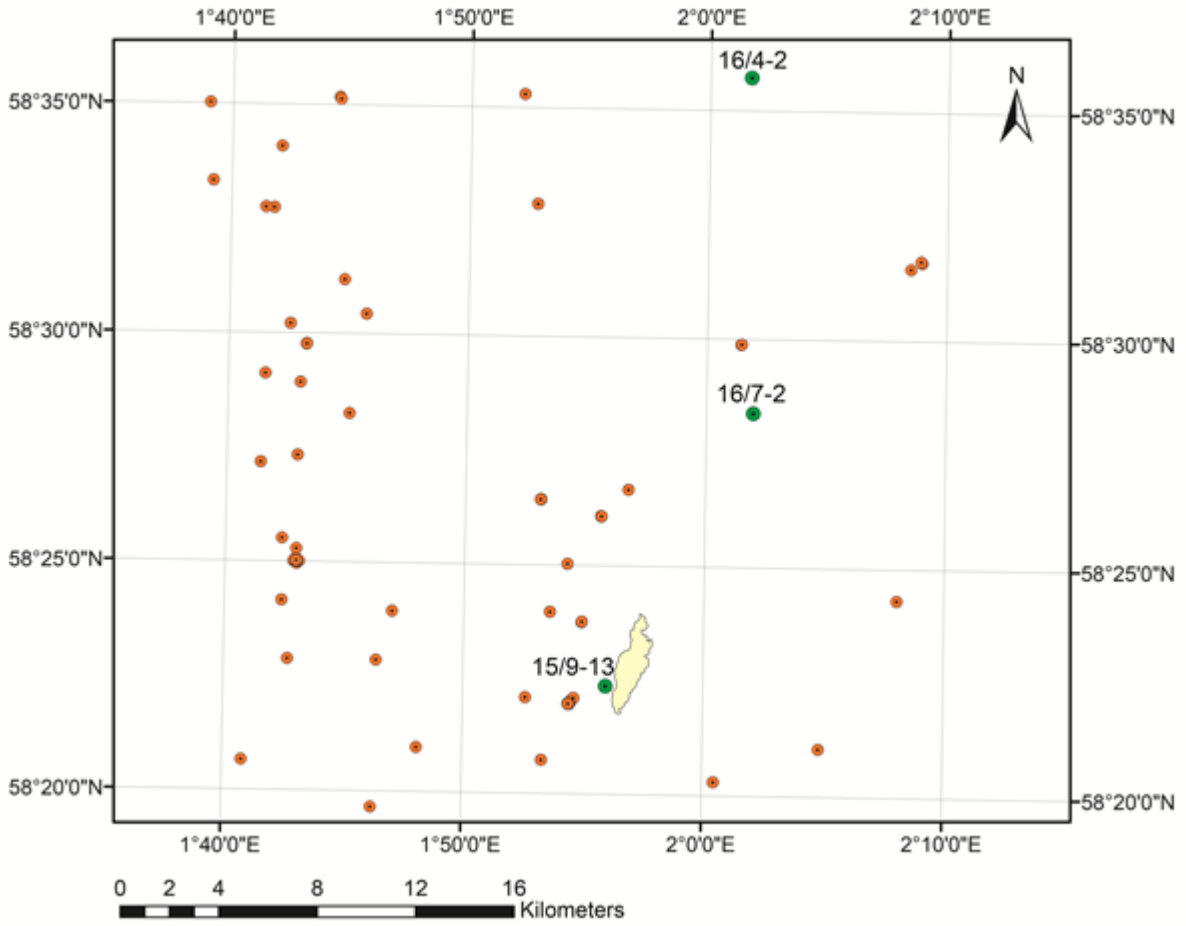

Fig. 36: Map showing the location of three investigated abandoned wells that are leaking methane (green dots), the location of other wells in that area (orange dots), and the extent of the subsurface CO_2 plume at Sleipner in 2008 (yellow).

Active bubble emissions released as single bubble streams and patchy bacterial mats were characteristic leakage features at the investigated wells. Direct gas flow measurements revealed a total seabed gas flow between 1 and 18.5 tons of CH_4 per year per well. The substantial variability of seepage activity is a result of significantly different numbers of total vents per well: 39 individual bubble streams were observed at well 16/7-2, whereas only 2 and 8 seep spots were found at wells 15/9-13 and 16/4-2, respectively. Total annual seabed emissions of all three wells of ~23 tons are similar to the natural seepage rates at Tommeliten (i.e. 26 t CH_4 yr^{-1}, Schneider et al., 2011), suggesting that leaky abandoned wells are an efficient source for methane into North Sea bottom waters.

A bubble size distribution was determined from video-analysis of seeping gas bubbles, combining 274 bubble size measurements at single bubble streams at well 16/4-2 and well 15/9-13 (Fig. 37). It is suggested to be representative for bubbles released from the fine to medium grained clayey sand found at the investigated wells.

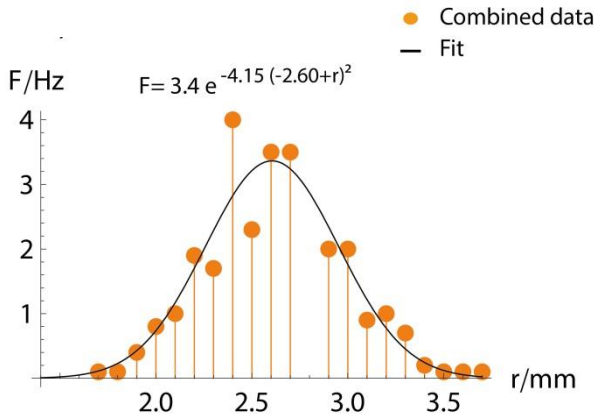

Fig. 37: Measured bubble release frequency (F) versus bubble radius (r), and Gaussian fit for the combined bubble size distribution based on measurements at single bubble streams at wells 15/9-13 and 16/4-2. The error, s^2, of the fit is 0.18 Hz.

3.3 Geochemical flux measurements

Marine systems are dynamic environments and this creates a number of problems in the monitoring and detection of any potential leakage from CCS sites. The modelled changes to the sediments and water column from leakage scenarios show a range of changes in the environment. The natural variation in CO_2 and pH in an area such as the North Sea is often greater than would result from a leakage, particularly under a diffuse chronic leak scenario. One way of accounting for this is to have a thorough understanding of the 'normal' environmental conditions, preferably over a number of seasonal cycles. One of the most useful means of achieving this is through the deployment of lander-based systems with suites of instrumentation. Currently off the shelf systems such as a recording current meter can be used with sensors for temperature and conductivity, this can go a long way towards constraining the natural variability in the physical environment, essential for inclusion in the models. With improvements in sensor technologies these lander-based, long-term deployments have the potential to provide essential information, both for baseline studies and for monitoring once operation at a site commences.

For these reasons, a lander system equipped with a series of sensors including conductivity, temperature, oxygen, hydrophones and flux meters was deployed at the site of the Hugin fracture during cruise JC77. The lander was recovered by a survey vessel from SubSea7 12 months later. An example of the data collected from these various sensors is shown in Fig. 5. Use of the NOC lander in the Central North Sea showed the natural variability in a number of physical factors essential for environmental modelling (Fig. 38).

The collection of data such as oxygen not only constrains the temporal variability within the marine environment, it is essential for some of the stoichiometric approaches currently used on for detecting land based CCS (Romanek et al., 2012), but are being investigated for use for marine CCS reservoirs. This unique data set represents the longest available time-series of data from the Sleipner area.

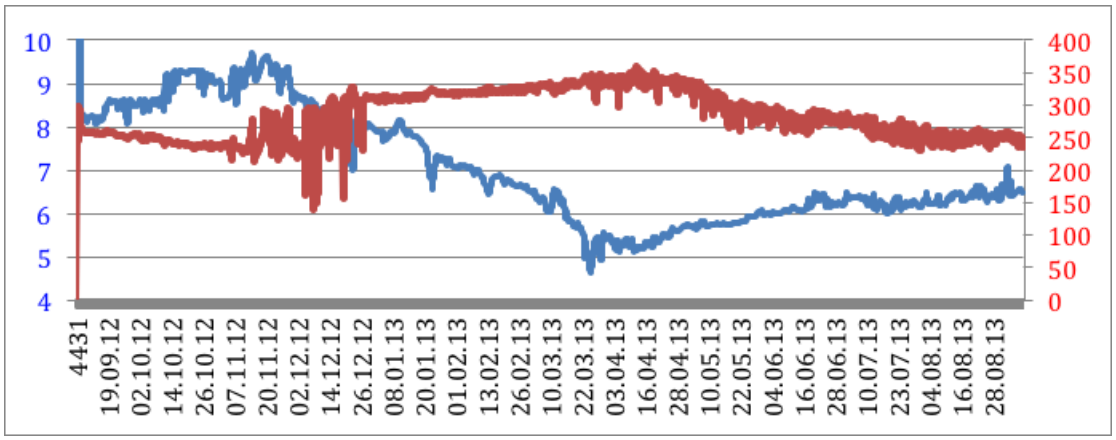

Fig. 38: Raw data from an Aanderaa Recording Current Meter (RCM) deployed on a seabed lander from September 2012 to October 2013. Blue (left axis) is temperature (°C) and red (right axis) is oxygen concentration (µmol L^{-1}).

This stoichiometric approach to characterize the differences in metabolism of background sediments versus sediments impacted by CO_2 and other geochemical species was applied by in situ flux measurements during short-term benthic lander deployments during GEOMAR cruises AL374 and CE12010 (Linke, 2011; 2012). During the BIGO deployments 4 samples were pumped at defined intervals into glass tubes to avoid the problem of dilution and to obtain uncontaminated samples from each of the 2 chambers. The glass tubes were directly connected to the inlet of a Membrane Inlet Mass Spectrometer to conduct the gas analysis. A linear decrease in oxygen was measured by optodes in all deployments, however, the sediments at the fracture were more active than at the abandoned well indicated by a steeper slope. As expected pCO_2 increased with time conversely to oxygen (Fig. 39).

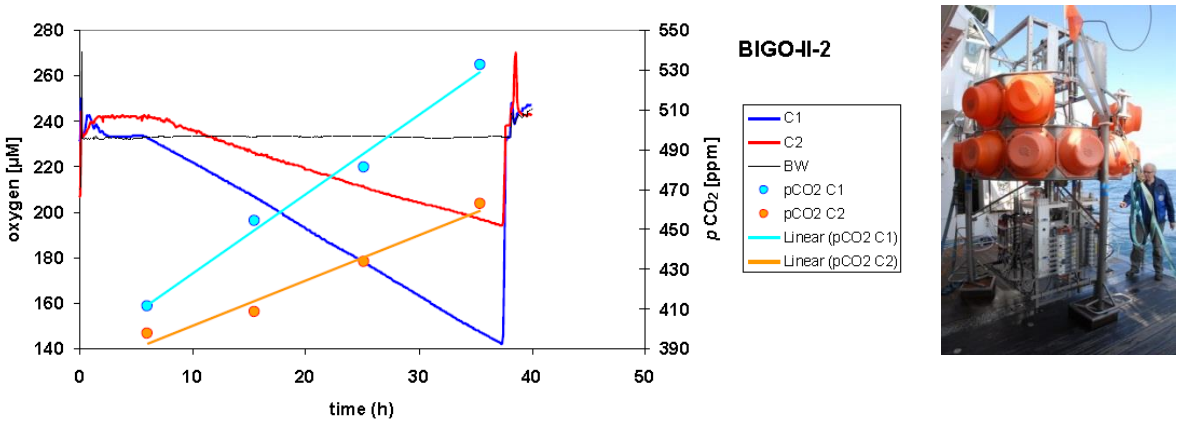

Fig. 39: Temporal evolution of pCO_2 (dots) and O_2 levels (lines) inside the benthic chambers C1 and C2 and the bottom water (BW) during BIGO deployment (right picture) at the fracture.

When looking at the molar ratios between oxygen uptake and the release of dissolved inorganic carbon (DIC) from the different sites, it is evident that the oxygen uptake is strongly enhanced while the molar ratio and the uptake of oxygen is diminished at the bacterial mat sites (Table 3). These observations imply that most of the enhanced oxygen consumption at bacterial mat sites is induced by AOM followed by aerobic sulfide oxidation. The methane flux from the subsurface fueling the excess oxygen consumption can be estimated from the flux data as 4 – 9 mmol m^{-2} d^{-1}.

Table 3: Benthic chamber measurements of oxygen uptake and release of dissolved inorganic carbon (DIC) at reference, abandoned well and Hugin fracture sites.

[mmol m^{-2} d^{-1}]	O_2 uptake	DIC release	DIC/O_2
Reference			
Chamber 1	4.6	4.8	1.04
Chamber 2	3.9	4.0	1.03
Well 15-9			
Chamber 1	11.1	8.4	0.76
Chamber 2	9.7	6.8	0.70
Hugin Fracture			
Chamber 1	22.9	11.5	0.50
Chamber 2	12.3	8.3	0.68

Furthermore, the measurements indicate that the molar flux ratio between natural respiratory CO_2 release and O_2 consumption might be a powerful tool to discriminate between highly variable CO_2 background fluxes (varying several orders of magnitude, see e.g. Luff and Moll, 2004) and minor CO_2 leakage fluxes as this ratio varies over a much narrower range. Enhanced flux ratios ($CO_2/O_2 >> 1$) would thus clearly indicate CO_2 leakage from the storage complex across the sediment/water interface while an increase in CO_2 fluxes accompanied by a corresponding rise in oxygen consumption could be ascribed to natural variability. Baseline and monitoring studies should thus rely on CO_2/O_2 flux ratios rather than highly variable and ambiguous CO_2 fluxes.

To assess the composition of the fluids that are seeping out along the Hugin Fracture, sediment pore waters were analysed at the fracture and in the background sediments (Fig. 40). Na , Cl and Mg contents of the fracture pore fluids were 10 - 15 % lower than those of the background pore fluid concentrations. Thus, a fluid distinct from seawater is seeping along the structure. To assess whether the seepage fluids may stem from the Utsira Formation, the pore fluid compositions were compared with compositional characteristics of Utsira Formation water. The Utsira Formation water is characterized by high Li (15 times background seawater concentration), B (3 times background seawater concentration), Na contents similar to background seawater and 40 % lower Mg concentrations than in background seawater as well as sulphate concentrations of only 10 µmol/l (background seawater concentrations are about 28 mmol/l). This is distinctly different from the sediment pore fluids. Instead the major element composition of the fracture pore fluids points towards fresh water input.

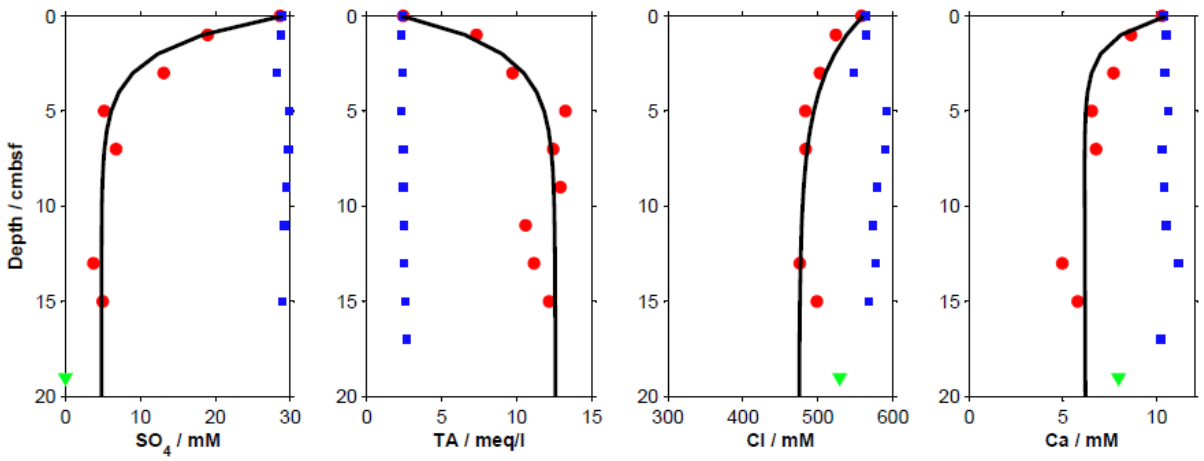

Fig. 40: Selected components of the push core porewater geochemistry suggest that the fracture is a conduit for upward flow of fresh water (red: fracture, blue: reference). Preliminary transport-reaction modelling estimates fluid advection velocities of ~50 cm/yr (black line). For comparison, the values for Utsira Formation (see also D2.1) water at Sleipner are also given (green).

Collection of sediment cores, especially relatively long cores, is invaluable in detecting and monitoring CO_2 leakage. To this end, we collected a series of vibrocores from the Sleipner area. Prior to cruise JC77, only short gravity cores (<1 m) had been collected from this area, and these indicated the upflow of methane rich fluids. However, the analysis of our longer (3 m) vibrocores shows that these fluids are in fact transported laterally, and not vertically (Fig. 41).

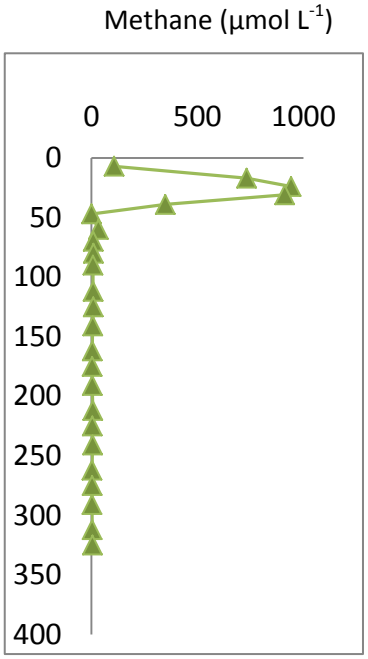

Fig. 41: An example of a long core taken as part of the ECO_2 study at the Hugin fracture indicating the methane is transported laterally.

Our geochemical analysis also reveal that the deep pore waters recovered both from the vicinity of the Hugin fracture, as well as from the area above the Sleipner CO_2 plume, show no evidence for

enrichment in Li or B, elements that are likely to be indicative of seepage of fluids from the Utsira Formation (Fig. 42).

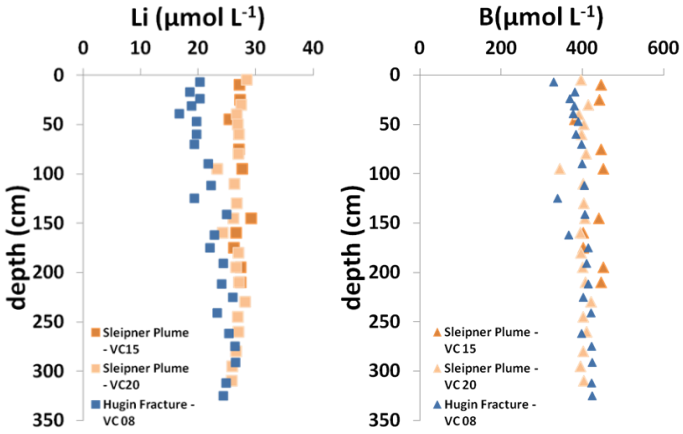

Fig. 42: Profiles of dissolved Li and B in pore waters from the Hugin fracture (blue) and from a region of the seafloor above the Sleipner CO_2 plume (orange) that is unaffected by fluid flow.

The vertical distribution of dissolved compounds in sediment cores, such as those shown in figures 41 and 42, can be used to model the flow rate of the pore water and/or gasses.

3.4 Impact of CO2 and other geochemical species on biological communities

Both, at the abandoned wells and at the Hugin fracture, fluid and gas flux foster the growth of bacterial mats. Further investigations at the Hugin fracture showed that the white bacterial mats have basically the same appearance at all the active spots, but show potentially different metabolisms. These range from sulfate reduction to sulphur oxidation to anaerobic methane oxidation. In the background sediments, aerobic ammonium oxidation was the prevailing mechanism.

4 Conclusions

- Natural analogues provide important insights into the key mechanisms and processes controlling CO_2 emissions, their fate and transport and their effects on marine biota.
- Furthermore, they are indispensable test grounds for leakage detection and monitoring tools and are ideal natural laboratories to evaluate the precision and operability of the instrumentation and the techniques involved.
- Unfortunately, two analogs (the Okinawa Trough and the Salt Dome Juist site) did not provide new results due to logistic reasons and the ephemeral and unpredictable occurrence of CO_2 anomalies, respectively.

•

5 References

Anzidei M. (1998). The marine digital terrain model of the Panarea Caldera Aeolian Islands, southern Italy. Annali di Geofisica 41(2): 265-270

Anzidei, M., Esposito, A., Bortoluzzi, G., De Giosa, F. (2005). The first high resolution bathymetric map of the exhalative area of Panarea (Aeolian Islands, Italy). Annals of Geophysics 48 (6): 17-39.

Arts, R., Eiken, O., Chadwick, A., Zweigel, P., van der Meer, L., and Zinszner, B. (2004). Monitoring of CO_2 injected at Sleipner using time-lapse seismic data. Energy 29, 1383-1392.

Buß, A. (2011), Plume disperal at hydrothermal vent fields with natural CO_2 seeps in the North-West Pacific, M.Sc. thesis, Institute of Environmental Physics, University of Bremen, Bremen, Germany

Caliro, S., Caracausi, A., Chiodini, G., Ditta, M., Italiano, F., Longo, M., Minopoli, C., Nuccio, P.M., Paonita, A., Rizzo, A. (2004). Evidence of a recent input of magmatic gases into the quiescent volcanic edifice of Panarea, Aeolian Islands, Italy. Geophys. Res. Lett. 31, L07619.

Chatwick, R.A., Zweigel, P., Gregersen, U., Kirby, G.A., Holloway, S., and Johannessen, P.N. (2004). Geological reservoir characterization of a CO2 storage site: The Utsira Sand, Sleipner, northern North Sea. Energy 29: 1371-1381.

Chadwick, R. A., Noy, D., Arts, R., and Eiken, O. (2009). Latest time-lapse seismic data from Sleipner yield new insights into CO_2 plume development. Energy Procedia 1, 2103-2110.

Chiocci, F. L., Bosman, A., et al. (2013). Bathy-morphological map. Eastern Aeolian Sector. Scale 1: 50 000. In: Lucchi, F., Peccerillo, A., Keller, J., Tranne, C. A, & Rossi, P. L. (eds) Geology of the Aeolian Islands (Italy). Geological Society. London. Memoirs 37: attached DVD.

Connelly, D.P. (2012): JC077 2nd – 28th 2012 cruise report, 64 pp.

de Beer, D., M. Haeckel, J. Neumann, G. Wegener, F. Inagaki, and A. Boetius (2013). Saturated CO_2 inhibits microbial processes in CO_2-vented deep-sea sediments. Biogeosciences, 10(8), 5639-5649, doi:10.5194/bg-10-5639-2013.

Esposito, A., Giordano, G., Anzidei, M. (2006). The 2002-2003 submarine gas eruption at Panarea volcano (Aeolian Islands, Italy): Volcanology of the seafloor and implications for the hazard scenario. Marine Geology 227, 119-134.

Gena, K., K. Kase, H. Chiba, and K. Nakashima (2005), Tin-bearing chalcopyrite and platinum-bearing bismuthinite in the active Tiger sulfide chimney, Yonaguni Knoll IV seafloor hydrothermal system, Okinawa Trough, Japan, *Eos Trans. AGU*, AGU Fall Meeting abstract #V51C-1492.

Graziani, S., Beaubien, S.E., Bigi, S., Lombardi, S. (2014) Spatial and temporal pCO_2 marine monitoring near Panarea Island (Italy) using multiple low-cost GasPro sensors. Environmental Science & Technology 48, 12126-12133, doi:10.1021/es500666u.

Gugliandolo, C., Italiano, F., Maugeri, T. (2006). The submarine hydrothermal system of Panarea (Southern Italy): biogeochemical processes at the thermal fluids - sea bottom interface. Annals of Geophysics 49 (2-3) 783-792.

Herreilers, H. (2012) Seafloor heterogeneities in the central North Sea: potential fluid migration pathways (Bachelor thesis), Christian-Albrechts-University, Kiel, 50 pp.

Inagaki, F., Kuypers, M.M., Tsunogai, U., Ishibashi, J., Nakamura, K., Treude, T., Ohkubo, S., Nakaseama, M., Gena, K., Chiba, H., Hirayama, H., Nunoura, T., Takai, K., Jørgensen, B.B., Horikoshi, K., Boetius, A. (2006) Microbial community in a sediment-hosted CO2 lake of the southern Okinawa Trough hydrothermal system. PNAS 103 (38), 13899-13900.

Kedzior, S., et al. (in prep.) Geochemical observations within the water column at the CO_2-rich hydrothermal systems Hatoma Knoll and Yonaguni Knoll IV, in the southern Okinawa Trough.

Konno, U., U. Tsunogai, F. Nakagawa, M. Nakaseama, J.-i. Ishibashi, T. Nunoura, and K.-i. Nakamura (2006), Liquid CO_2 venting on the seafloor: Yonaguni Knoll IV hydrothermal system, Okinawa Trough. Geophys. Res. Lett., 33(16), L16607, doi:10.1029/2006gl026115.

Leighton, T.G. and White, P.R. (2012) Quantification of undersea gas leaks from carbon capture and storage facilities, from pipelines and from methane seeps, by their acoustic emissions. Proceedings of the Royal Society A, 468, 485-510. (doi:10.1098/rspa.2011.0221).

Leifer, I., and Boles, J. (2005) Measurement of marine hydrocarbon seep flow through fractured rock and unconsolidated sediment. Marine and Petroleum Geology 22: 551-568.

Linke, P. and Schmidt, M., eds. (2010) Fluid and gas seepage in the North Sea, RV Celtic Explorer/Cruise Report CE0913: Fluid and gas seepage in the North Sea: Bremerhaven - Bremerhaven, 26.07. - 14.08.2009. IFM-GEOMAR Report, 36. IFM-GEOMAR, Kiel, 82 pp.

Linke, P., ed. (2011) RV ALKOR Fahrtbericht / Cruise Report AL374; 29.05.-14.06.2011, Kiel - Kiel ; ECO2 - Sub-seabed CO2 Storage: Impact on Marine Ecosystems. IFM-GEOMAR Report, 51. IFM-GEOMAR, Kiel, 55 pp.

Linke, P., ed. (2012) RV Celtic Explorer EUROFLEETS cruise report CE12010 - ECO2@NorthSea: 20.07. – 06.08.2012, Bremerhaven - Hamburg. GEOMAR Report, N. Ser. 004, Kiel, Germany, 60 pp.

Linke, P., ed. and shipboard scientific party (2014) RV POSEIDON Fahrtbericht / Cruise Report POS469: 02. - 22.05.2014, (Bari, Italy – Malaga, Spain) “Panarea” Panarea shallow-water diving campaign 10. – 19.05.2014. GEOMAR Report, N. Ser. 019, GEOMAR, Kiel, Germany, 50 pp.

Linke, P., Schmidt, M., Rohleder, M., Al-Barakati, A., Al-Farawati, R. Novel online digital video and high-speed data broadcasting via standard coaxial cable onboard marine operating vessels (submitted to Marine Technology Society Journal).

Luff, R., Moll, A. (2004). Seasonal dynamics of the North Sea sediments using a three-dimensional coupled sediment-water model system. Continental Shelf Research 24: 1099-1127.

McGinnis, D. F., Schmidt, M., DelSontro, T., Themann, S., Rovelli, L., Reitz, A., Linke, P. (2011a). Discovery of a natural CO_2 seep in the German North Sea: Implications for shallow dissolved gas and seep detection. J. Geophys. Res. 116: C03013.

McGinnis, D., Beaubien, S. E., Bigalke, N., Bryant, L. D., Celussi, M., Comici, C., De Vittor, C., Feldens, P., Giani, M., Karuza, A., Schneider von Deimling, J. (2011b). The Panarea natural CO2 seeps: fate and impact of the leaking gas (PaCO2). R/V URANIA. Cruise No. U10/2011. 27 July – 01 August 2011. Naples (Italy) – Naples (Italy) EUROFLEETS Cruise Summary Report. IFM-GEOMAR. Kiel. 55 pp. DOI 10.3289/CR_ECO2_19835.

Monecke, T., Petersen, S., Hannington, M. D., Anzidei, M., Esposito, A., Giordano, G., Garbe-Schönberg, D., Augustin, N., Melchert, B., Hocking, M. (2012). Explosion craters associated with shallow submarine gas venting off Panarea Island. Italy Bulletin of Volcanology 74(9): 1937-1944.

Morgan, E., Hauton, C., Schade, H., Melzner, F., Guilini, K., Vanreusel, A., Meyer, S., Ramette, A., Dupont, S. and Widdicombe, S. (2014) Report on marine species: The response and potential adaptation of marine species to CO2 exposure associated with different potential CO2 leakage scenarios. ECO2 Deliverable D4.2, 113 pp.

Neumann, J. (2012), Effect of high CO2 and low pH on benthic communities of the deep sea, PhD thesis, Department of Biology and Chemistry, University of Bremen, Bremen, Germany

Rehder, G., and J. Schneider von Deimling (2008), RV Sonne Cruise Report SO 196 SUMSUN 2008, Leibniz Institute for Baltic Sea Research Warnemünde, Warnemünde.

Romanak, K.D., Bennett, P.C., Yang, C.B., Hovorka, S.D. (2012). Process-based approach to CO2 leakage detection by vadose gas monitoring at geologic CO2 storage sites. Geophys. Res. Lett. 39. doi. 10.1029/2012GL052426.

Sakai, H., T. Gamo, E. S. Kim, M. Tsutsumi, T. Tanaka, J. Ishibashi, H. Wakita, M. Yamano, and T. Oomori (1990a), Venting of carbon dioxide-rich fluid and hydrate formation in Mid-Okinawa Trough backarc basin, Science, 248(4959), 1093-1096, doi:10.1126/science.248.4959.1093.

Schmidt, M., Linke, P., Sommer S., Esser D., Cherednichenko, S. Natural CO2 seeps offshore Panarea – A test site for subsea CO2 leak detection technology (submitted to Marine Technology Society Journal).

Schneider von Deimling, J., Rehder, G., Greinert, J., McGinnis, D.F., Boetius, A., Linke, P. (2011). Quantification of seep-related methane gas emissions at Tommeliten, North Sea. Continental Shelf Res. 31, 867-878.

Shitashima, K., Y. Maeda, Y. Koike, and T. Ohsumi (2008), Natural analogue of the rise and dissolution of liquid CO_2 in the ocean, Int. J. Greenh. Gas Control, 2(1), 95-104, doi:10.1016/s1750-5836(07)00092-8.

Streif, H. (2002), Nordsee und Küstenlandschaft – Beispiel einer dynamischen Landschaftsentwicklung, Akad. Geowiss. Hannover, Veröffentl., 20: 134 – 149.

Tassi, F., Capaccioni, B., Caramanna, G., Cinti, D., Montegrossi, G., Pizzino, L., Quattrocchi, F., Vaselli, O. (2009). Low-pH waters discharging from submarine vents at Panarea Island (Aeolian Islands, southern Italy) after the 2002 gas blast: Origin of hydrothermal fluids and implications for volcanic surveillance. Applied Geochemistry 24, 246-254.

Vielstädte, L., Karstens, J., Haeckel, M., Schmidt, M., Linke, P., Reiman, S., Liebetrau, V., McGinnis, D.F., Wallmann, K., (submitted). Quantifications of methane emissions at abandoned gas wells in the Central North Sea. (Journal of Marine and Petroleum Geology)

Wenzhöfer, F., Asendorf, V., Grünke, S., Hagemann, J., Hoge, U., Hovland, M., Lehmenhecker, S., Shurn, K., Weiz, E., Wulff, T., (2012). Cruise Report HE 377, 16 – 24 April 2012, Bremerhaven – Bremerhaven, 20 pp.

Yanagawa, K., Morono, Y., de Beer, D., Haeckel, M., Sunamura, M., Futagami, T., Hoshino, T., Terada, T., Nakamura, K., Urabe, T., Rehder, G., Boetius, A., and Inagaki, F. (2012) Metabolically active microbial communities in marine sediment under high-CO2 and low-pH extremes. ISME doi: 10.1038/ismej.2012.124

Acknowledgement

The research leading to these results has received funding from the European Community's Seventh Framework Programme (FP7/2007-2013) under grant agreement no 265847.